Analysis of Inductive Coupling Wireless Power Transfer Systems

Arianna Ginette Amaya Colina
`ar0727am-s@student.lu.se`

Department of Electrical and Information Technology
Lund University

Academic Supervisor: Professor Buon Kiong Lau (bkl@eit.lth.se)

Industrial Supervisor: Laurens Swaans (ls@nok9.com)

Examiner: Professor Mats Gustafsson (mats.gustafsson@eit.lth.se)

September 14, 2018

Abstract

Inductive coupling wireless power transfer (WPT) technology is gaining increasing popularity in recent years, especially in the field of wireless charging of portable devices. Although the principles behind WPT systems can be explained using well known results from electromagnetic theory, many questions remain regarding the behavior of such systems. This thesis focuses on identifying and analyzing the most important parameters of such system, with emphasis on the coupling factor. Algorithms to calculate the coupling factor and other parameters based on mathematical models of physical phenomena are developed and presented. This algorithm development is also called the analytical approach. For the coupling factor part, a commercial electromagnetic simulation software (Ansys Maxwell) was selected to validate the results obtained from the corresponding algorithm and also evaluate the performance of general-purpose simulators suitable for use in this field. For other WPT system parameters, the algorithm was compared to the results from LTspice. The results obtained from the developed algorithms and simulations are compared to measurement results collected from real transmitter and receiver coils. The results show that both the analytical and simulation approaches can provide estimated parameter values of interest that are close to the empirical values, with percentage error being in the low single digits in most scenarios. However, the developed algorithms are more specialized, and hence easy to implement and computationally more efficient. Consequently, they can be used to generate larger amounts of data for detailed analysis and characterization of WPT systems with relative ease.

Popular Science Summary

Wireless charging is a popular new feature for electronic devices such as smartphones and tablets. This technology eliminates the need of carrying multiple power adapters and cables. What's more, wireless chargers can be embedded in furniture in places such as hotels, restaurants and libraries, and clients need only take out their devices and put them in a designated spot to charge them. The same wireless power transfer (WPT) technology has also been used in other applications such as powering kitchen appliances and charging electric vehicles. Due to the growing interest in this field, it is important to clearly understand the relationship between the different parts of WPT systems.

This thesis project focuses on identifying the most important parameters of WPT systems and studying how such systems respond to changes in any one of these parameters. The emphasis is on the coupling factor, which measures how much of the energy transmitted reaches the receiving device. The thesis work was commissioned by nok9 AB, a Swedish company with headquarters on Malmö that builds and sells the equipment used to verify if wireless chargers comply with the Qi Specification, which is the dominant wireless charging standard today. For this study, relatively simple algorithms are developed analytically based on mathematical models of WPT systems. Commercial simulators are also used for comparison. Simple real systems are also built, and the parameters under study are measured, to validate the analytical and simulation results.

The data collected are presented in graphical forms, to show how WPT systems respond to changes in parameters such as relative position of transmitter and receiver coils, input voltage, as well as receiver and transmitter coil geometries. Comparison with measurements shows that both simulations and the proposed analytical methods achieve acceptable accuracy on most occasions. This is important, because it demonstrates that the relatively simple algorithms of the analytical approach can be successfully used to study WPT systems. They could be used to decrease the cost associated to developing new devices, by reducing the reliance on building prototypes. Furthermore, the algorithms developed in this thesis project can be as accurate as commercial simulation software, and can be faster to run for the cases considered in this study. However, the current version of the algorithm for coil parameter calculation cannot take into account the presence of other objects. Similarly, the algorithm for calculating WPT system behavior assumes a simplified WPT system. These limitations present opportunities for future work

in this field.

Table of Contents

List of Figures

x

List of Tables

Introduction

1.1 Background

Wireless power transfer (WPT) or wireless power transmission refers to any energy transmission method in which the receiving and transmitting devices are not connected using wires. The first experiments regarding WPT are usually attributed to Nikola Tesla, the famous Serbian-American inventor. Tesla wanted to distribute energy wireslessly all over the globe. Although he did not manage to do so, he did succeed in demonstrating a few early WPT systems. According to contemporary press, he managed to light two 50 watts incandescent lamps, 42 kilometers away from the transmitting station [1]. Interest in the field increased after World War II . A key event was the 1964 demonstration of a microwave based system used to power a small helicopter, such that it did not need to land to refuel. This experiment introduced the rectenna, or rectifier antenna, a component later used in many systems [2]. William C. Brown did some modifications on the original rectenna, and his 0.1 square meter version got NASA's attention. The agency funded several studies in the field, with the goal of applying the technology to solar energy collection [2].

With the exception of Tesla's experiments, all of these studies dealt with what is known as far-field WPT, in which energy is transmitted via electromagnetic radiation (e.g. microwaves or light). Although far-field WPT has proven useful in high power military, industrial and space applications, it is not without drawbacks. On the technical side, it requires very efficient power sources and rectifiers for the transmitter and receiver, and beam-forming antennas. Historically, cost of development and deployment has been high. Safety is also a concern, due to the risk of exposure to high levels of radio frequency electromagnetic radiation [3].The aforementioned limitations make using this technology in consumer applications unfeasible.

On the other hand, WPT is becoming very popular for consumer applications today. It is used for charging cellular phones, smart watches, laptops, tablets and others small size devices. However, it is near-field WPT, in which energy is transformed through electrodynamic or electrostatic induction, which is used in these cases. In fact, the application of near-field WPT has been extended to charging or powering other electronic devices such as blenders, mixers and other kitchen devices, as well as higher-power machines such as electric cars [3].

Due to the rapidly-growing popularity and fast increase in the number of use cases of near-field WPT technology, the need arose to design a standard that would allow compatibility between different devices. The most popular one is the Qi Specification. The Qi Specification is developed and promoted by The Wireless Power Consortium (WPC) [4]. WPC is a worldwide organization supported by more than 600 companies. The Qi WPT system uses inductive and resonant coupling technologies. Inductive power transmission systems consist of two inductive coils, one of them called the power transmitter (PTx) coil and the other called the power receiver (PRx) coil. These coils are magnetically coupled. Therefore, when an alternating voltage is applied to the PTx coil, a voltage is induced on the PRx coil [5]. It is common to use resonant circuits in inductive coupling transmission systems due to the resulting improvement in the transferred power [6].

The Qi Specification establishes the allowed power levels, the operating frequency range, coupling requirements, communication protocol and other details necessary for the correct operation of near-field WPT systems. The Specification is divided into four parts. The first part covers the electrical, mechanical and thermal characteristics of both PTx and PRx coils, and this part is called Primary Interface Definition in the Qi Specification. The second part, called Secondary Interface Definition, establishes the requirements and limitations of the interface between the WPT system and its environment. The third part is called Compliance Testing and it is only available to WPC members. The last part contains examples, to help design power transmitters and power receivers. Parts 1, 2 and 4 are also available as a published standard by the International Electrotechnical Commission (IEC).

The current version (1.2.3 public version and 1.2.4 member version) of the Qi Specification allows for fast charging (transmission and reception of up to 15 watts of power), foreign object detection and an identifier for power receivers (WP-ID) [7].

1.2   Motivation

When compared to the traditional wired power approach, WPT brings many benefits. It can eliminate the, sometimes hazardous, messes of cables in homes and offices. Restaurants, hotels and airports can use this technology to allow their clients to charge their smartphones everywhere without having to carry chargers or power banks around. Furthermore, it deals with the problem of having to own and carry several incompatible cables, which is useful for travelers. And these benefits do not only apply to smartphones: the market for wireless charging (and powering, in general) is growing and it includes wearable devices such as smart watches, smart eyewear and others devices for health and fitness purposes. The basic principles behind inductive coupling have been well studied. It can be explained using Faraday's law of electromagnetic induction. However, many interesting research questions remain concerning the design and optimization of inductive coupling WPT systems. As these systems become more common, it is important to understand them in detail.

Half of the thesis work is focused in a specific variable of these systems: the

coupling factor or coupling coefficient.The coupling factor is determined by the physical configuration of a PTx coil and a PRx coil. Even with the exact same PTx and PRx coils, the coupling can be different every time the devices are paired, due to different relative coil positionings. With a standard like Qi there are many different PTx and PRx product executions from different manufacturers. Every unique combination of these PTx and PRx products can give a different coupling factor. That makes coupling very important to understand as a WPT parameter.

1.3 Goals

The main goal of this thesis is to analyze WPT systems. This is achieved by:

- Analyzing how the coupling factor, one of the key parameters of WPT system, responds to changes in other parameters such as the relative position between coils, coil size and coil shape.

- Developing a method to calculate the coupling factor between two coils. There are many studies on this subject, specifically on how to calculate it using the relationship between mutual inductance, self-inductances and coupling factor as well as applying integration methods. In this project, the focus is on developing a method to calculate the coupling factor between coils of arbitrary geometries.

- Identifying other key parameters of WPT systems through modeling and parametric studies.

- Modeling the coils and full WPT systems using electromagnetic simulation software.

- Validating the methods and models developed through hardware implementations and measurements.

1.4 Structure

This report is divided into 5 chapters, including this introductory one. The following chapter details the mathematical framework used to study WPT systems, presenting the models and equations that will be referenced throughout the rest of the document. Chapter 3 describes the methodology used in the study. It contains sections describing the numerical algorithms developed from the mathematical models, as well as the simulation models and real systems built in order to evaluate the accuracy of the algorithm. Chapter 4 presents the results obtained from the three approaches mentioned and compares them. Finally, the report ends with the conclusions derived from these results and a discussion of possible future work.

Theoretical Framework

This chapter covers the theory behind the electric circuit and magnetic field phenomena studied in this thesis. It starts with an explanation of the terms from electromagnetic theory that the reader needs to know in order to understand the concepts involved in the study of WPT systems. A brief description of energy transfer methods follows, with emphasis on inductive coupling, the method studied in this project. Then, the electric circuit issues behind a general WPT system will be described. After that, the usual method used to analytically calculate the coupling factor will be explained.

2.1 WPT Systems

When studying WPT systems, the most important part is the energy transfer method used. As mentioned before, inductive or magnetic power transfer is one form of energy transfer through free space using electromagnetic (EM) fields. Energy transfer methods are usually classified in two categories: far-field and near-field. In the case of far-field methods, electromagnetic radiation is used. This type of WPT is also called "beamed power transmission" [2], because it relies on directional antennas for efficient energy transmission and reception. Common radiation types used are microwaves and light. On the other hand, near-field methods refer to energy transmission via electromagnetic induction. This category is further subdivided depending on the type of field used to induce energy. If electric fields are used it is electrostatic induction, and if magnetic fields are used it is electrodynamic induction. Again, there are two types of electrodynamic induction: inductive coupling and magnetic resonant induction [8].

Inductive coupling consists of transferring energy through magnetic fields and can be explained using Ampere's circuital law, Faraday's voltage induction law and Lenz's law. Ampere's circuital law establishes that a current-carrying conductor produces a magnetic field. Faraday's law states that if the magnetic flux changes with time, a voltage is induced in any conductor placed in the vicinity of the source inductor. And, according to Lenz's law, "the polarity of the voltage is such that a current is generated on closing a circuit whose induced magnetic field opposes the original magnetic field" [9].

In an inductive coupling WPT system, energy is transfered from the PTx coil, which carries a current (I) that generates a magnetic field ($\mathbf{B}$). The target coil,

PRx, is placed close to this coil. Figure 2.1 shows a basic system, where each coil is a filamentary loop. In real systems the transmitter, the receiver or both coils can be spiral coils, have multiple layers and different geometries (circular and rectangular being the most common ones). Some transmitters can even be composed of more than one coil. The magnetic field generates a current in the second coil. The magnetic flux amount transferred depends on the coupling between the two coils, and this flux generates the mutual inductance. Part of the flux of the primary coil does not link to the second one, and generates leakage inductance (L_l) [9]. Another concept to keep in mind is magnetized inductance (L_m), which is used to analyze circuits with transformers. This will be explained later in this section.
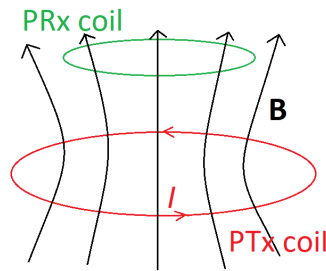
Figure 2.1: Basic model of inductive coupling.

Besides inductive coupling, there is also the concept of magnetic resonant induction. In this case the transmitter, the receiver, or both, are resonant circuits. A resonant circuit is formed by a combination of inductance, capacitance and resistance. Figure 2.2 shows a basic model of this type of circuits, with an inductor (of inductance L), a capacitor (of capacitance C) and a resistor (with resistance R). It is a series resonance circuit. This type of circuits have a current behavior like the one shown in Figure 2.4. The current is maximum at the resonant frequency, which is reached when the total reactance of the circuit is zero. Some important definitions in this part are:

The capacitive reactance is given by:

$$X_C = -\frac{1}{\omega C} \tag{2.1}$$

The inductive reactance is given by:

$$X_L = \omega L \tag{2.2}$$

The reactance is zero when the magnitude of the inductive reactance is equal to the magnitude of the capacitive reactance, because they cancel each other due to the phase difference being 180 degrees.

The resonant frequency of a circuit like the one shown in Figure 2.2 is given by:

$$\omega_o = \frac{1}{\sqrt{LC}} \tag{2.3}$$

Another important concept in resonant circuits is the quality factor represented by Q. The quality factor is the ratio of the energy stored in reactive components
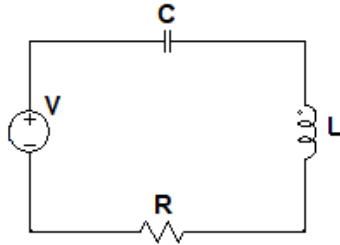
Figure 2.2: Magnetic resonant induction circuit model.
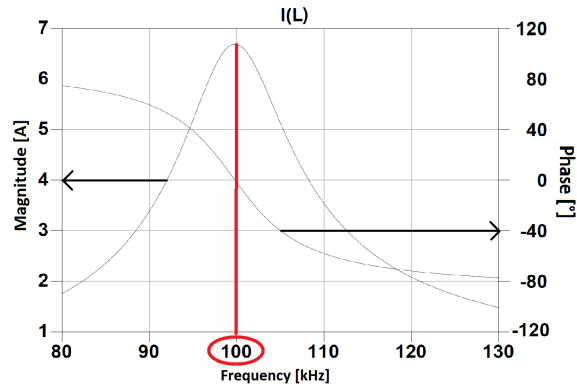
Figure 2.3: Resonant circuit's current.

of the circuit to the amount of input energy dissipated as heat in the circuit. The Q value is given by:

$$Q = \frac{X_L}{R} \tag{2.4}$$

Figure 2.4 depicts the current flowing through the inductor as a function of frequency for several resistances. A high Q value results in a narrower curve, in other words, a more selective circuit. When R is smaller the Q value is higher, and vice versa.
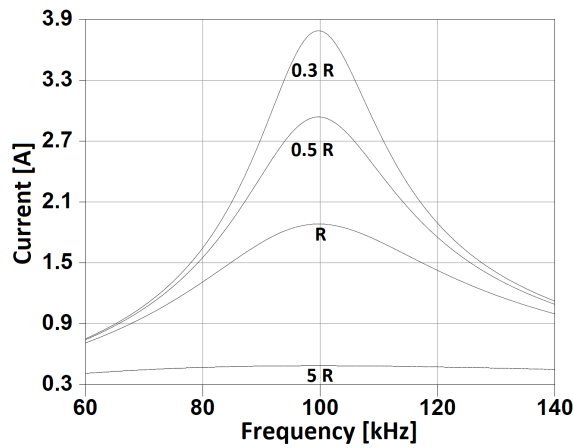
Figure 2.4: Resonant circuit's current with different R values.

When the transmitter's resonant frequency is equal to the receiver's resonant frequency then the frequency at which the transmitter can transfer the highest power coincides with the one at which the receiver can receive the highest power. Resonant coupling is used in wireless power transmission to improve the amount

of power transmitted in comparison to only inductive coupling. The use of resonant circuits allows for an increase in the range of operation, which is useful for applications such as portable device chargers, where there is a separation distance between the transmitter coil and receiver coil. For this reason any Qi transmitter and receiver work in inductive coupling and resonant coupling modes. An example of devices where only inductive coupling is used are electric toothbrushes.
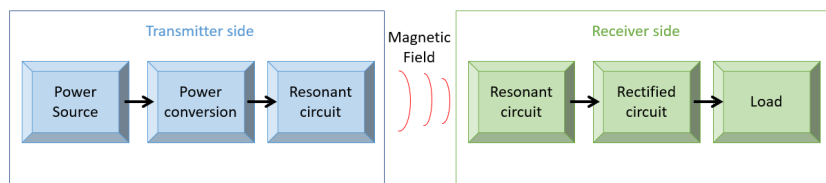
Figure 2.5: Block diagram of a WPT system.

Real inductive coupling WPT systems have a complex structure. Figure 2.5 gives a block diagram of this type of systems. Note this is a simplified version and circuits used to communication between the transmitter and receiver are not considered. The transmitter side can be divided into three blocks. The first one represents the power supplier and voltage regulators needed to feed the resonant circuit. The second one comprises the circuits needed to convert the power supplied to the signal desired, either by modifying its frequency or magnitude. In the real case, the input signal shape is usually square because it is easier to generate a square wave than a sinusoidal wave. This part includes a half bridge or full bridge inverter. The last block represents the resonant circuit formed by the coil, a capacitive element whose value is the one necessary to get the desired resonant frequency and a resistive part that represents the circuit losses. The receiver side is formed by a resonant circuit, a rectified circuit and the load. The rectified circuit can comprise of diodes or switches. This circuit changes the polarity of the input signal to positive or negative. In some cases, a smoothing capacitor is added after the rectifier step. This capacitor is used to store energy and it discharges slowly, which reduces the signal ripple and leads to a smooth DC output voltage. Figure 2.6 illustrates a common setup for this type of circuits.

For theoretical reasons, a simplified circuit will be used in this project. This is also referred to as the First Harmonic Approximation (FHA) model. Thus model only considered the fundamental frequency and simplified passive components. This circuit scheme is displayed in Figure 2.7. It is formed by a primary and a secondary resonant circuit, a power source and a load. Each resonant (RLC) circuit comprises of a coil (L), a capacitor (C) and a resistor (R) that represents the equivalent series resistance (ESR). The subindex p or s indicates if the component belongs to the primary or secondary side.

2.1.1   Equivalent model

The transmitter and receiver coils together form a transformer. Therefore, the equivalent circuit model used in the analysis of transformers can be used. In
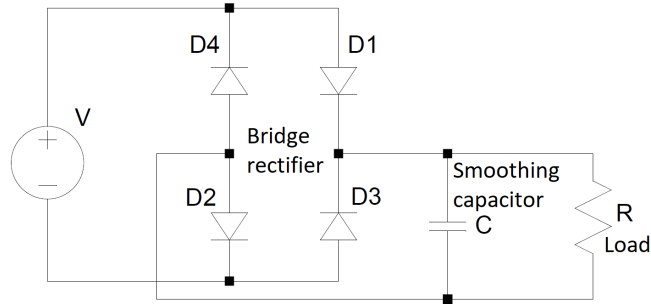
Figure 2.6: A common rectified circuit
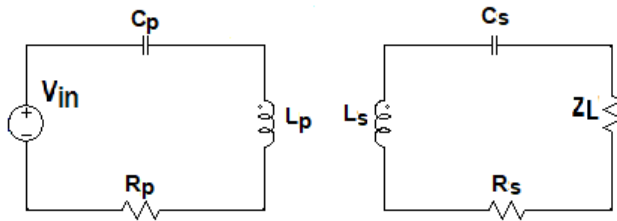
Figure 2.7: Simplified WPT model

this case there is no core and the air gap length is larger than for traditional transformer, then the leakage flux will be higher. A model which considers leakage inductance must be used. This equivalent model is displayed in Figure 2.8. To arrive at this model one needs to convert the transformer created by L_p and L_s in the original model into a "T" equivalent circuit using the magnetizing inductance (L_m) and the leakage inductances (L_{Lp} and L_{Ls}). It is also necessary to add the reflected impedances that represent the secondary side, with an apostrophe added to each of these terms to differentiate them from the original parameters in Figure 2.8. This model was taken from [10].
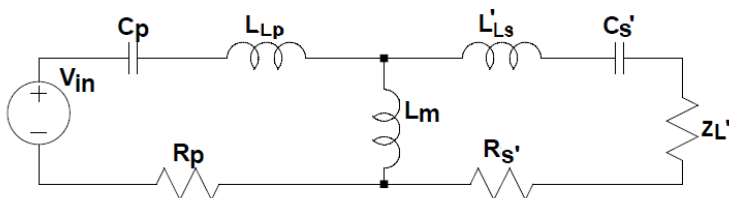
Figure 2.8: Equivalent WPT model

In this case, the turns ratio is given by:

$$n = \sqrt{\frac{Ls}{Lp}} \qquad (2.5)$$

The magnetizing inductance is given by:

$$L_m = kL_p \qquad (2.6)$$

where k is the coupling factor for the given coil configuration. The coupling factor will be explained in detail in the next section. The leakage inductance is given by:

$$L_{Lp} = L_p(1 - k) \qquad (2.7)$$

$$L_{Ls} = L_s(1 - k) \qquad (2.8)$$

Reflected impedances

Besides leakage inductances and magnetizing inductance, an ideal transformer is added to the model used for transformers [11]. Reflected impedances must be used to take this voltage transformation into account in the equivalent circuit. The primary side variables remain the same, but the secondary side impedances seen by the primary circuit must be calculated. The impedances from the secondary side (denoted with apostrophe) will appear as n^2 times lower on the primary side:

$$L'_{LS} = \frac{1}{n^2}(L_{LS}) \qquad (2.9)$$

$$C'_S = \frac{1}{n^2}(C_S) \qquad (2.10)$$

$$R'_S = \frac{1}{n^2}(R_S) \qquad (2.11)$$

$$Z'_L = \frac{1}{n^2}(R_L) \qquad (2.12)$$

The equivalent model simplifies the derivation of mathematical equations, which in turn facilitates the study of the dependencies between variables analytically and numerically.

The following equations can be derived using the equivalent model:

- Load voltage vs. input voltage

$$V_L = V_{in}Z_L\sqrt{\frac{L_p}{L_s}}\frac{skL_p}{Z_s + skL_p} \qquad (2.13)$$

where Z_p is the impedance seen by the primary source and is given by

$$Z_p = \frac{1}{sC_p + sL_p(1 - k) + Z_s \parallel Z_{lm} + R_p} \qquad (2.14)$$

$Z_s \parallel Z_{lm}$ is the impedance of magnetizing inductance in parallel with the receiver impedance. Z_s is given by

$$Z_s = \frac{s^2 L_p L_s C_s (1-k) + s C_s (Z_L + R_s) L_p + L_p}{s L_s C_s} \qquad (2.15)$$

Z_{lm} is given by

$$Z_{lm} = s L_m \qquad (2.16)$$

and s is defined as

$$s = j\omega \qquad (2.17)$$

- Primary current vs. load resistance

$$I_p = \frac{V_{in}}{Z_p} = V_{in} \left(L_p \frac{s^3 L_s C_s k (1-k) + s^2 C_s k (Z_L + R_s) + sk}{s^2 L_s C_s + s C_s (Z_L + R_s) + 1} \right) \\ + V_{in} (s C_p + s L_p (1-k) + R_p) \quad (2.18)$$

- Primary current vs. coupling factor

$$I_p \quad = \quad \frac{V_{in}}{-k^2 s^2 L_s \frac{A}{B} + k\left((s R_s + s Z_L + \frac{1}{C_s})\frac{A}{B} - s L_p\right) + C} \quad (2.19)$$

where A, B and C are given by

$$A = C_s L_p^2 \qquad (2.20)$$

$$B = s C_s L_p L_s + C_s L_p R_s + C_s L_p Z_L + \frac{Lp}{s} \qquad (2.21)$$

$$C = s L_p + R_p + \frac{1}{s C_p} \qquad (2.22)$$

These equations were chosen because they show the mathematical relation between parameters which were studied in a real experimental setup. They were taken from the same internal document where the model was defined and verified.

2.2 Coupling Factor

As was said before the magnetic flux amount transferred from the PTx coil to the PRx coil depends on the coupling between the coil inductors. How much the coils are coupled is expressed by the coupling factor, commonly represented by k. This parameter takes values between 0 and 1, where k equals to 1 means maximum coupling. k depends on many variables. From previous works, it is well-known that the coupling factor decreases when the distance z between the coils is increased. The k factor also depends on the geometry of each coil, that is the coil shape, number of turns, number of layers, space between turns and relative dimensions of each coil. Common k values are between 0.3 to 0.6 [12].

The coupling factor is defined by the following equation [13]:

$$k = \frac{M}{\sqrt{L_p L_s}} \tag{2.23}$$

where M is the mutual inductance and L_p and L_s are the self-inductances of the PTx and PRx coils.

The value of M depends on the coils' respective geometries and their positions relative to each other. To get this value the well-known Neumman's formula for mutual inductance can be used. This formula is given by [14]:

$$M = \frac{\mu_o}{4\pi} \oint_{C_s} \oint_{C_p} \frac{dl_p dl_s}{r} \tag{2.24}$$

where dl_p and dl_s correspond to differential lengths of the paths that describe each coil, r is the distance from each dl_p to each dl_s and μ_o is the permeability of vacuum, which is equal to $4\pi \times 10^{-7}\mathrm{H/m}$.

There are many previous studies based on numerically solving Equation (2.24). Some values are tabulated in [15]. In [15], only consider the following geometries are considered: circular filaments, circular coils of rectangular cross section and solenoids.

Other more recent works derive closed form solutions for circular filaments arbitrarily positioned in space using the method of vector potential (e.g. [16]), or the equations for magnetic force [17]. All of these approaches use the elliptical integrals to solve the problem.

In the case of coaxial circular filamentary conductors the solution of this integral is given as a function of the elliptical integrals [14]:

$$M = \mu_o \sqrt{ab} \left[\left(\frac{2}{c} - c \right) K(c) - \frac{2}{c} E(c) \right] \tag{2.25}$$

where a and b are the radii of the two coils, h is the vertical (z) distance between them, $K(c)$ and $E(c)$ are the complete elliptic integrals of the first and second kind. They are given by:

$$K(c) = \int_0^{\pi/2} \frac{1}{\sqrt{1 - (\sin(\phi)c)^2}} h\phi \tag{2.26}$$

$$E(c) = \int_0^{\pi/2} \sqrt{1 - (\sin(\phi)c)^2} h\phi \tag{2.27}$$

$$c = \sqrt{\frac{4ab}{(a+b)^2 + h^2}} \tag{2.28}$$

The solution of equation (2.24) in the case the filamentary conductors with lateral misalignment is given by [14]:

$$M_L = \frac{\mu_o ab}{2\pi} \oint_{C_p} \frac{\cos\beta}{\sqrt{ab_L}} G(r) d\phi \tag{2.29}$$

where

$$G(r) = \left(\frac{2}{r} - r\right)(r) - \frac{2}{r}E(r) \tag{2.30}$$

$$r = \sqrt{\frac{4ab_L}{(a + b_L)^2 + h^2}} \tag{2.31}$$

$$b_L = \sqrt{b^2 + d^2 + 2db\cos\phi} \tag{2.32}$$

$$\tan\beta = \frac{d\sin\phi}{b + d\cos\phi} \tag{2.33}$$

and d is the lateral distance between the axes of the two coils and variable ϕ represents the angular displacement used to describe the current path on the second coil.

From these examples the reader can deduce that the complexity of these solutions increases when more complex cases are considered. For example, the solution in the angular misalignment case is more complex than the ones shown above. Another issue with this type of solutions is that they are only applicable to specific geometry types (mainly circular ones). If the shape of one of the coils is rectangular, a common shape in product implementations of WPT systems, the solutions presented above are not valid.

Another important aspect in the analysis of WPT systems is how much the coupling factor changes in the presence of materials, either an increase when a material like ferrite is placed over one or both coils or a decrease when a metal like aluminum is placed between the two coils. Examples of previous works on this topic are [18] and [19]. Both studies propose that the mutual impedance between two inductors is the sum of the mutual impedance without the metal plus the impedance due to the presence of the metal [19]. The decrease in coupling factor due to the presence of metals is due to the phenomenon of eddy currents. When metals are placed in the vicinity of the transmitter coil, the alternating magnetic field generated by this coil will produce eddy currents in the metal. This current generates a magnetic field that opposes the exciting magnetic field. Therefore the magnetic field which affects the receiver coil will be the source magnetic field minus the eddy current field. This phenomenon decreases the efficiency of the system. On the other hand, when materials with very large permeability (e.g. ferrite) are placed at the bottom of a coil, the magnetic field transmitted is increased due to the ferrite redirecting most of the magnetic field to the coil's top side.

Methodology

Three methodologies or approaches to analyze the parameters were used in this project: analytical, simulation and measurement. These are applied to both coupling factor and WPT system analyses. The first approach consists of doing direct analysis on the parameters based on the theory behind each phenomenon. The second part consists of creating models using specialized software to simulate the parameters' behaviors and validate the theoretical results. The last part is used to confirm the results from the first two by comparing them to the practical, real case. The tools and software used are explained in the following sections.

3.1 Coupling factor

3.1.1 Analytical approach

The PTx and PRx coils used in WPT systems can have many different geometries. One of the goals of the project was to develop a general analytical method to compute the coupling factor between two current paths when geometries and positions are known.

As was said in Section 2.2, previous works focused on giving a closed form formula to get the coupling factor (k). That becomes impractical when the coils have different geometries because it is necessary to solve integral (2.24) for each geometry. Moreover, closed form expressions may not be possible when irregular geometries are needed, and when it becomes important to also consider the terminals (feed lines) to the coils. For this reason, the goal in this project was to develop a more general and practical method. The method developed is based on solving the aforementioned integral numerically. The tool used to achieve it is MATLAB®. This is a well known programming platform and language used in science and engineering. The MATLAB language is matrix-based, which simplifies implementing math heavy algorithms [20]. For detailed information about the MATLAB platform, the reader can consult its online documentation [21].

The algorithm implemented to numerically perform the integral consists on splitting the current path into small pieces (differential element in length) and evaluating the integrand in expression (2.24) for each differential length. In this way, any coil geometry and even the terminals can be taken into consideration.

To account for the presence of plates of other materials placed "behind" a coil,

the method from [19] was employed. However, this can only be used with planar circular coils. The following equation is used:

$$M_{total} = j\omega M + Z_t \tag{3.1}$$

where M_{total} is the mutual inductance, Z_t is the contribution from the plate, ω is the angular frequency, and M is the mutual inductance without taking the plate into account. Z_t is calculated using the method described in [19], but it does not account for coil terminals. M is calculated using the algorithm described in this section instead, which takes in account the coil terminals. Therefore, some error is expected in calculating M_{total}, since Z_t had not been modified to include the effect of the coil terminals.

The algorithm's inputs are: the coil's shapes and the separation between them. This separation is represented by d and h values for the horizontal and vertical planes, respectively (see Figures 3.1 and 3.2). The shape is represented by a list of 3-dimensional coordinates (i.e. a discretization of the real shape). Since circular, spiral and square coils are common, the program can generate the coordinate list automatically if the user selects one of these shapes and specifies some related parameters. For example, if a spiral coil is desired its shape in 2D polar coordinates is modeled by the Archimedean spiral equation (3.2). Here a and b are real numbers that determine how many turns the spiral has and the distance between turns [22].

$$r = a + b\theta \tag{3.2}$$

Real coils have terminals to connect to the power source (or load), and in some simulation software such as LTspice®, sink terminals are necessary for magnetic simulations. With the implemented algorithm, there is a lot of flexibility when describing the overall shape of each coil, which makes it easy to consider the contributions from the coil terminals. In order to find out if these terminals impact the variables under study, the algorithm was executed with and without them and the results were compared to the measured values.
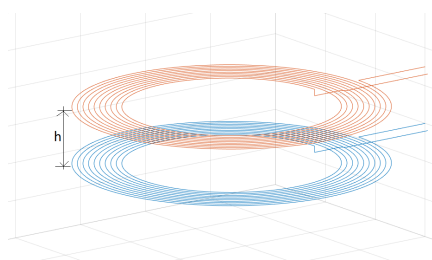
Figure 3.1: Vertical distance h between coils

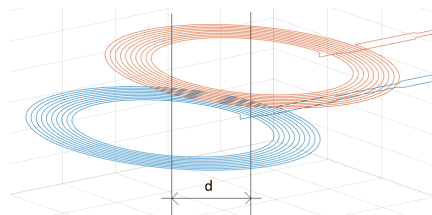Figure 3.2: Horizontal separation (or lateral displacement) d between coils' central axes

To calculate the coupling factor using equation (2.23), the self-inductance of each coil has to be determined first. The formula to get the the self-inductance follows the same mathematical idea as the one for mutual inductance, and thus the same algorithm is used to calculate it. The main difference is that both current

paths are the same (since the flux going through the coil with the flux-generating current is of interest). One problem with reusing the mutual inductance algorithm is that integral (3.13) has a singularity when $r = 0$. Therefore to calculate the self-inductance it is necessary to run this algorithm for several small values of h instead of 0, and with those results the value when $h = 0$ is numerically approximated by extrapolation.

3.1.2 Simulation approach

Simulators enjoy widespread use in the electronics design space, both in industry and academia, because they can be used to find out the characteristics of the designed devices without investing the money needed to built prototypes that may not work. They allow visualization of how the components react to variations in different parameters, like applied voltage and frequency. They are also used to change physical, electrical and magnetic characteristics of the device under study and then to reassess its performance. Thus, engineers can make more informed decisions when selecting materials and choosing between competing designs. Nowadays, many software packages for electromagnetic field simulation are available. Some examples are COMSOL Multiphysics, CST EM STUDIO® and ANSYS Maxwell®. The last one was chosen to validate the values from the analytical approach.

Ansys is a comprehensive program for 3D design and simulations in the fields of fluids, electronics, semiconductors, structural analysis and embedded software, among others. The electronics suite can simulate antennas, automative radars, RF and microwaves, low-frequency electromagnetics, power electronics and others. Ansys Maxwell, used during this thesis work, was developed for static, frequency-domain (low frequency) and time varying electromagnetic and electric field simulation. It contains several solvers, including the magnetostatic and eddy currents solvers used in this project [23].

The magnetostatic solver, as its name implies, assumes the magnetic field is constant. This makes it less accurate than the eddy currents solver for low frequency cases, but it is more computationally efficient. The frequency range used during the experiments is around 100 kHz. In this range, the wavelength is around 3 kilometers, calculated using the relation $\lambda = \frac{\nu}{f}$ where ν and f are the phase speed (i.e., $3 \times 10^8 m/s$ in vacuum) and the frequency of the wave. The maximum distance between the coils considered was 15 mm, which is very small when compared to the wavelength, so the magnetostatic solver's assumption is reasonable and thus it can be used. However, this solver was not accurate enough to study the effects of metals placed close to the coils. The eddy currents solver was used for this kind of scenarios. This solver computes steady-state, time-varying (AC) magnetic fields at a given frequency. For the most part, the same models defined for use with one solver can be reused for the other, and only new excitation sources had to be defined.

After choosing the correct solver, the next step is to create the structure to be simulated. The base structures considered were based on predefined structures included in the program. There is a library of common materials such as copper, ferrite, FR4, etc. The calculation domain for the simulation was marked

with a vacuum box surrounding the structure. DC current sources were used as excitations for each coil when the magnetostatic solver was selected, and AC current sources were used with the eddy currents solver. The simulations had to be fine tuned in order to run them on the available computer resources, due to high memory usage. For example, the mesh was modified to be finer in the regions containing the coils and coarser in the rest of the calculation domain.

Models to calculate both the self-inductance and the mutual inductance were built, and will be explained in detail in Section 3.1.2. In Ansys Maxwell the user can specify sets of values for variables and run simulations for each value in the set without having to manually redefine the model for every value, and this functionality was used extensively in the mutual inductance case. Like in the analytical approach, two variables were defined: h and d, which represent the vertical distance and the lateral displacement, respectively. Figure 3.3 shows several instances of the same model obtained by changing the value of h.

(a) $h = 2.45$mm.

(b) $h = 5$ mm.

(c) $h = 10$ mm.

(d) $h = 15$ mm.
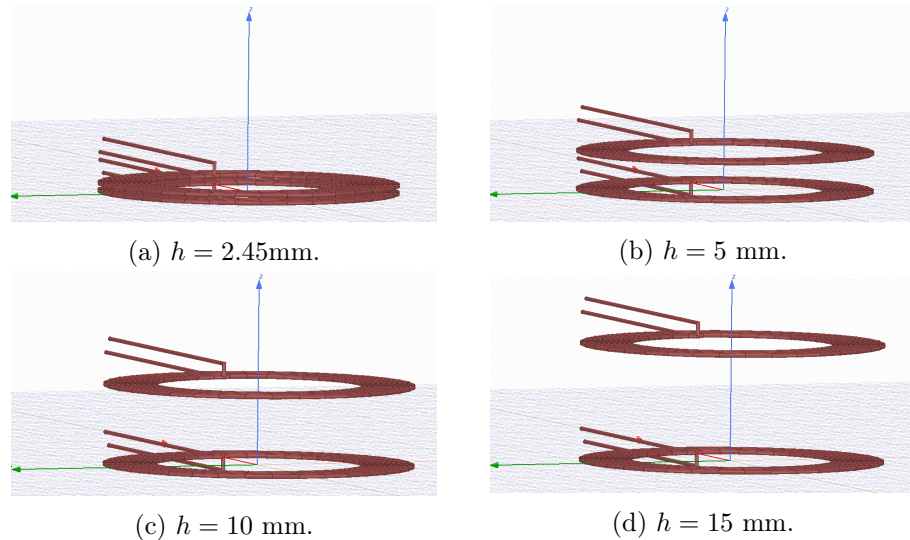
Figure 3.3: Different Ansys Maxwell models obtained by varying a parameter. In this case the vertical distance (h) is changed.

For more information about modeling and simulation using Ansys Maxwell, the reader should check the Ansys Maxwell Getting Started Guides or the Maxwell Online Help. These materials can be accessed from the software.

Description of magnetics simulations

This section shows some example simulations built with Ansys Maxwell for the purpose of evaluating different quantities (e.g., self and mutual inductances). Each model consists of a description, a list of related coil parameters and a figure. The first two models, designed to calculate self-inductances, were built to evaluate the performance of the simulator and learn how to use it.

I) Self-inductance (Magnetostatic solver)

(a) Square coil

A square coil (on PCB) was built to validate the performance of the simulator with a geometry different from the traditional circular shape. The coil is shown in Figure 3.4. The materials selected for the coil are the same as the ones used for flexible PCBs. That is, the coil metal is made from copper (of bulk conductivity 5.8×10^7 S/m) and the rest of the board from polyamide (of relative permitivity 4.3 and dielectric loss tangent 0.004). Other physical characteristics are listed below:

- Inner radius: 19.5 mm
- Turns: 8
- Wire thickness: 0.5 mm
- Space between turns: 0.5 mm
- Size of PCB: 150 mm $\times$ 90 mm
- Thickness of PCB: 0.05 mm

(b) Spiral coil with ferrite

This is a two-layers spiral coil with a thin ferrite plate in the bottom. The conductor is made from copper and the dimensions of the coil correspond to the Qi Specification for TPT2 [24]. Figure 3.5 shows the resulting model.
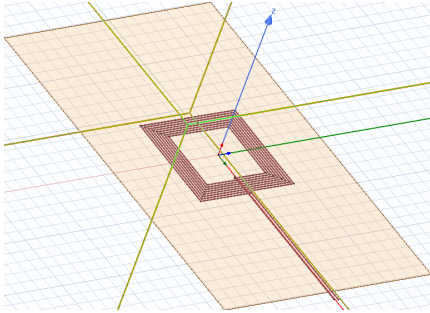
Figure 3.4: Model to calculate self-inductance of a square coil.
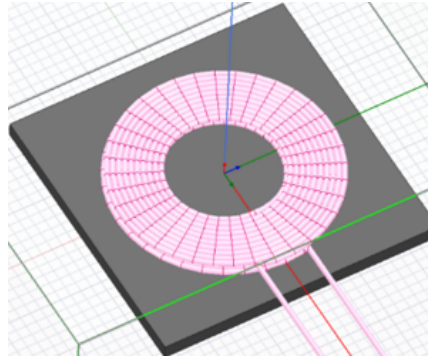
Figure 3.5: Model to calculate self-inductance of a coil on a ferrite plate.

II) Mutual inductance (Magnetostatic solver)

(a) One loop coil: The one-loop case is only interesting as a theoretical exercise, since it is unlikely to be found in real systems due to its low inductance. Two examples were analyzed. The first one (see Figure 3.6) corresponds to the scenario when the wire thickness is 0.5 mm. Then the wire thickness was increased to 0.7 mm, to study how wire thickness affects the mutual inductance and validate the analytical approach. The conductors were made from copper and their radius was 20 mm. The separation distance between the two coils in Figure 3.6 is 5 mm.
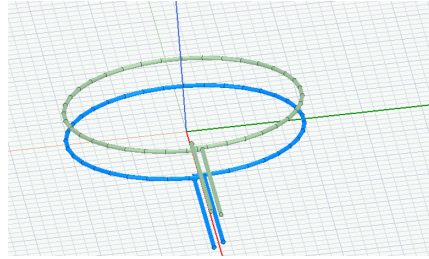
Figure 3.6: Model to calculate mutual inductance between two one-loop coils.
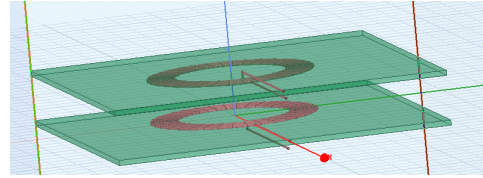
Figure 3.7: Model to calculate mutual inductance between two spiral coils. Each one has 10 turns.

(b) Spiral coil: Figure 3.7 shows the 3D model created in Ansys to get the mutual inductance between two spiral coils on PCBs. Copper was selected as the material for all coils, and they had an FR4 plate in the bottom, to simulate some PCB coils that were built to compare the simulations with real measurements. More details about the physical coils are included in Section 3.1.3.

III) Mutual inductance (Eddy current solver) As was explained before, some simulations were done to investigate how the coupling factor changes when there are metals close to the coils. If we want to study the effect of external materials the eddy currents solver must be used. This simulation model is based on Type 1 coils (with the distance between the coils being 3 mm). The dimensions of Type 1 coils will be given in Section 3.1.3. A flat metal cylinder was added between the coils, and it has the following characteristics:

- Metal: Aluminium
- Relative permeability (μ_r): 1.000021
- Bulk conductivity: 3.8×10^7 S/m
- Diameter: 2 mm
- Height: 2.90 mm

Figure 3.8 shows the resulting model.

3.1.3   Measurement approach

In order to validate the analytical and simulation approaches described earlier, real models were built to collect measurements for comparison. The purpose of this section is to describe the coils built to study the coupling factor behavior and the procedure used to collect measurements. Four different spiral coil types were used, with the purpose of observing the changes in the coupling factor from reasons other than changing the relative position of the coils. For example, the different types enable an evaluation on how the coupling factor reacts to changes in the number of loops or the coils' dimensions. Some measurements were realized
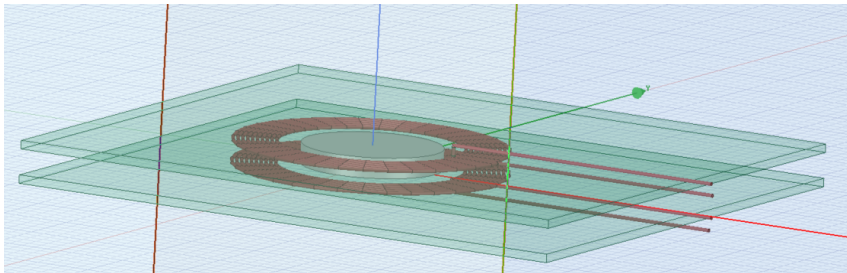
Figure 3.8: Model to calculate mutual inductance in presence of
an aluminium cylinder.

with square coils to analyze how the algorithm works with other geometries than
circular coils.

Materials and Equipment

1. PCB circular spiral coils
   It was essential to control the vertical distance between two coils and the
   horizontal distance (or lateral displacement) between the axes of two coils,
   and to be able to repeat experiments under the same conditions. At first,
   the coils were made using wires, but the measurement results were unstable.
   Therefore, PCB coils were built instead, using spacers to adjust the rela-
   tive positions between two coils. Thus, the positions could be modified as
   necessary and the coils kept in place for any number of measurements. Mea-
   suring using coils with a single or a few turns would be useful for evaluating
   how well the algorithm performs in each scenario. As was said before, four
   different coil types were considered. Their characteristics are listed below:

   - Coil Type 1

     Maximum outer radius: 20
     Number of turns: 10
   - Coil Type 2

     Maximum outer radius: 20
     Number of turns: 1
   - Coil Type 3

     Maximum outer radius: 20
     Number of turns: 10
   - Coil Type 4

     Maximum outer radius: 10
     Number of turns: 1

   All of the types share the following characteristics:

   - Spacing between turns: 0.178 mm

- Track width: 0.5 mm
- Copper thickness: 0.2 mm
- Substrate material: FR4

Note that the copper thickness is included in the radius (i.e. the radius is measured from the center of the coil to the most distant edge of the wire). When trying to simulate the coils or to calculate the coupling factor analytically, half of the wire thickness has to be substracted from the radius so that the filamentary wire model aligns with the center of the wire instead.

The choice of track dimensions is based on having a geometry as close as possible to the one used in the simulation models, as well as achieving constant current density. Ideally, track width and wire thickness would be equal, but 0.5 track width and 0.2 wire thickness was the best option offered by the PCB manufacturer.

Figure 3.9 shows the PCB coils designed for this project.

(a) Type 1

(b) Type 2

(c) Type 3

(d) Type 4
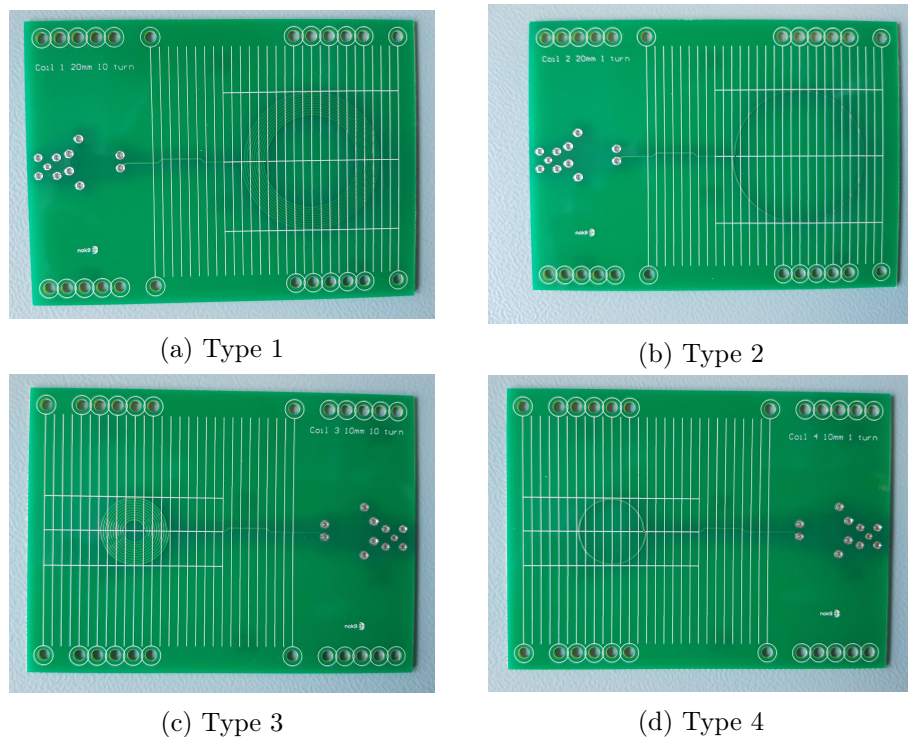
Figure 3.9: PCB circular spiral coils designed.

2. PCB square spiral coil

   Outer diameter: 42 mm

   Spacing between turns: 0.5 mm

Track width: 0.5 mm

copper thickness: 0.035 mm

Number of turns: 8

Substrate material: Polyamide

Figure 3.10 shows the PCB square spiral coil used.
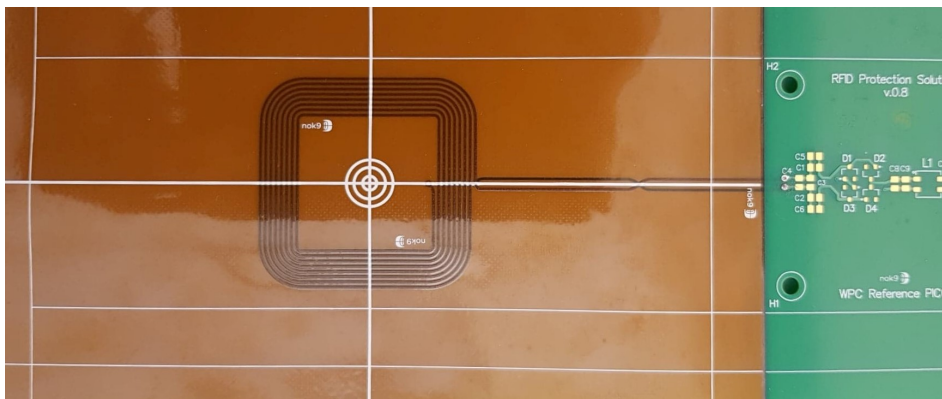
Figure 3.10: PCB square spiral coil

3. LCR meter

Two different tools were used to measure the necessary values, in order
to be able to verify them by comparing the two reported values. Since
measurements on different equipment are always slightly different, this also
ensures that the algorithm developed is not biased towards a particular tool.
Measurements were also repeated with two pairs of coils, to minimize the
impact of errors in the physical setups.

The LCR meter were used to get measurements are:

- GW-Instek LCR-8101G
- Keysight Technologies E4980A

4. Ferrite plates

- Size: 106×106 or 53×53
- Relative magnetic permeability: 2300
- Resistivity: $500\Omega.\text{cm}$

Procedure

Four measurements were needed to get the coupling factor between two coils:

- The primary coil inductance when the secondary coil is in open circuit.
- The secondary coil inductance when the primary coil is in open circuit.

- The equivalent inductance when L_p and L_s are in series-aiding configuration.

- The equivalent inductance when L_p and L_s are in series-opposing configuration.

The voltage used is 500 mV and the frequency is 100 kHz for all measurements.

To calculate mutual inductance one starts from the equations for two inductors in series (terminal voltages for a two-coil system) [25]:

$$v_1 = j\omega L_{11} i_1 + j\omega L_{12} i_2 \tag{3.3}$$

$$v_2 = j\omega L_{21} i_1 + j\omega L_{22} i_2 \tag{3.4}$$

where $L_{12} = L_{21} = M$ is the mutual inductance.

Figure 3.11 shows two inductors in series-aiding and series-opposing configuration. The equations for each case are:

In series-aiding configuration:

$$i_2 = i_1 \tag{3.5}$$

$$v_{aid} = v_1 + v_2 \tag{3.6}$$

$$v_{aid} = j\omega L_{aid} i_1 \tag{3.7}$$

In series-opposing configuration:

$$i_2 = -i_1 \tag{3.8}$$

$$v_{opp} = v_1 - v_2 \tag{3.9}$$

$$v_{opp} = j\omega L_{opp} i_1 \tag{3.10}$$

From the equations for the first configuration it can be shown that [25]:

$$L_{aid} = L_{11} + 2L_{12} + L_{22} \tag{3.11}$$

And from the equations for the second one [25]:

$$L_{opp} = L_{11} - 2L_{12} + L_{22} \tag{3.12}$$

From equations (3.11) and (3.12), the mutual inductance is given by:

$$M = \frac{L_{aid} - L_{opp}}{4} \tag{3.13}$$

Figure 3.11: Left: Inductors in series-aiding configuration. Right: Inductors in series-opposing configuration.

3.2 WPT systems

A similar framework as for studying coupling factor was used to study WPT systems. First, an analytical approach to represent the system based on the existing theory was developed. Then, a simulator was chosen, to see how well the analytical approach compares with a simulation approach. Finally, a real system was built to collect measurements for comparison with the results from the analytical and simulation approaches.

3.2.1 Analytical approach

The equations corresponding to the equivalent model presented in Section 2.1.1, were used to build a MATLAB® script to study WPT.

The *tf* command from the Control System Toolbox® was used to create the polynomial transfer function of the system [26]. After that, the *bode* command was used to generate data to create a bode plot [27]. This command takes a set of frequencies and the transfer function as input and returns the magnitude and phase of the function's response.

In the developed script the user needs to specify the frequency range, number of sample for that frequency range, input voltage, inductance of the coil, capacitor value and ESR value for both the primary and secondary sides (R_p and R_s), the load value and the system's coupling factor. These values are used to calculate the primary and secondary resonance frequencies and the quality factor of each side. The transfer function is created using the relations for leakage inductances and magnetizing inductance given in Section 2.1.1 and applying the reflected impedance concept. All system variables can be plotted. The primary coil current (I_p) and the load voltage (V_L) were of special interest for this project and were compared with the values obtained from the real system. Figure 3.12 shows an example output from the script, when the input parameters are given by the following values:

$f_{min} = 50$ kHz, $f_{max} = 150$ kHz, $V_{in} = 3$ V, $C_p = 0.486 \times 10^{-6}$ F, $L_p = 5.14 \times 10^{-6}$ H, $R_p = 0.0391$ Ω, $C_s = 0.491 \times 10^{-6}$ F, $L_s = 5.10 \times 10^{-6}$ H, $R_s = 0.0396$ Ω, $Z_L = 10.5$ Ω, $k = 0.656$.

Resonance split

A Python script was written to find out the minimum load value at which the resonance split phenomenon does not occur. The scripts uses a computer algebra library to find the expression for primary coil current as a function of load starting
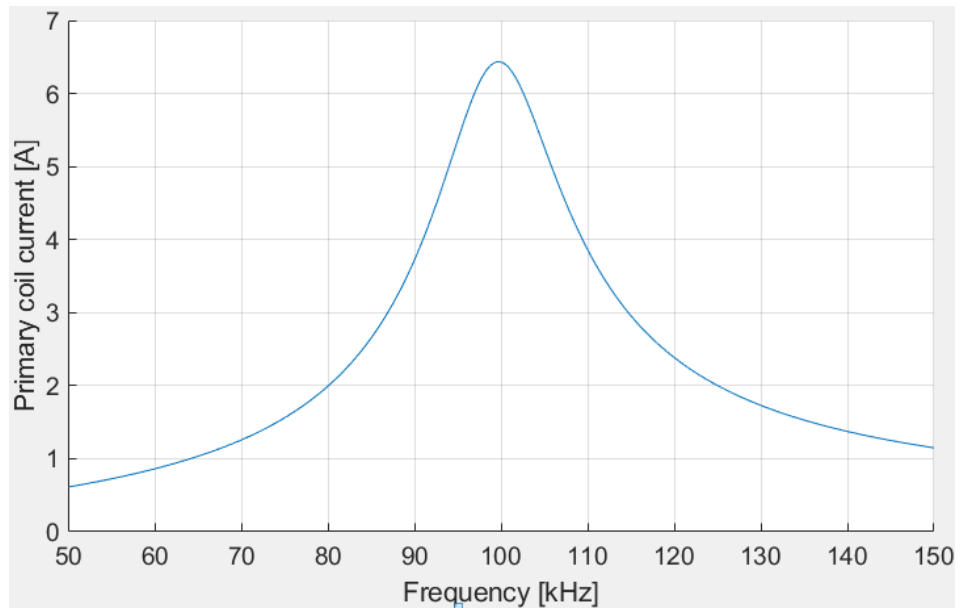
Figure 3.12: Waveform from MATLAB script corresponding to
the primary coil current.

from the same equations used to model the WPT system. The derivative of the
expression is found, in order to find its stationary points. If resonance split has not
occurred, the expression will have a single real positive stationary point, a global
maxima. If the phenomenon does occur, it will have three real positive stationary
points instead, corresponding to two local maxima and a local minima in between.
Thus, one can analytically determine if resonance split occurred by counting the
number of such points. The numerator of this derivative is a polynomial of degree
56, so it's roots can only be found numerically. The script repeats this procedure
for a sequence of load values, to find the point in which the number of local maxima
changes. Note that this method does not only count the local maxima, but it also
finds the frequencies at which they (and the local minima, if it exists) occur.

3.2.2   Simulation approach

The second approach used to analyze WPT system behavior was simulations us-
ing LTspice®. LTspice is a SPICE (Simulation Program with Integrated Cir-
cuit Emphasis) simulation program developed at Linear Technology (now part of
Analog Devices) [28]. With this tool analog circuits can be modeled with the
schematic/symbol editor and the signals through the circuit can be analyzed us-
ing the waveform viewer. The software has a library with common components
such as resistors, inductors, capacitors and others. It includes functionalities for
multiple types of analysis, such as transient analysis, AC analysis, DC sweep and
stochastic noise analysis [29]. For this investigation the first two types were used.
   Figure 3.13 shows a generic inductive coupling WPT system modeled using

LTspice. Using the K-statement, the program allows easy modeling of transformers [30]. The parameters used in this directive are the primary coil inductance, the secondary coil inductance and the coupling factor.
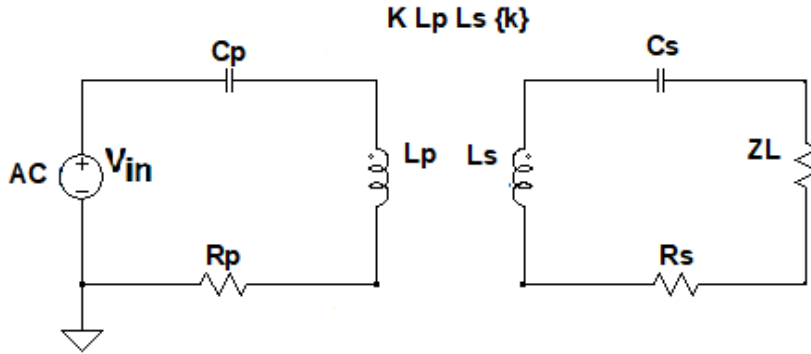
Figure 3.13: LTspice model of a generic WPT system.

Figure 3.14 shows the primary coil RMS current obtained from LTspice with the same parameters as those used in the previous section.
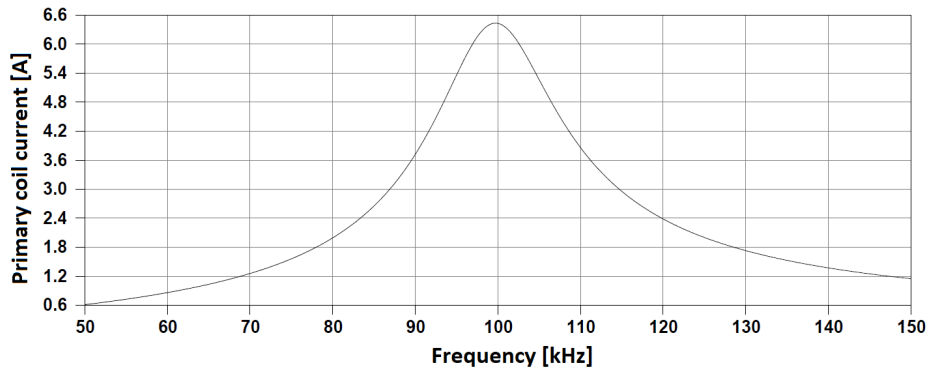
Figure 3.14: Waveform from LTspice corresponding to the primary coil RMS current.

3.2.3   Measurement approach

The final part of the project involved taking measurements of a real WPT system. This section describes the setup and materials used.

The first step was creating resonant circuits for the transmitter and receiver sides. The PCB coils described in Section 3.1.3 were used. However, Types 2, 3 and 4 were not used for this WPT system study due to their low inductance. This is an issue because if the inductance is low, the mutual inductance will be low as well, which in turn means the voltage induced in the secondary side will

be low. This is problematic because measuring a low signal is more error prone. Another problem with using these coils is that the resonant frequency chosen for each resonant circuit was 100 kHz, because this is within the frequency region used by all Qi devices. The corresponding inductances for the coils were around 5 μH for Type 1, 0.2 μH for Type 2, 1.3 μH for Type 3, 0.1 μH for Type 4. To create a circuit that resonates at 100 kHz, it is necessary to use a larger capacitance, around 0.49 μF for Type 1, 11.5 μF for Type 2, 1.8 μF for Type 3, 20 μF for Type 4. Components with such high capacitance are uncommon. NP0 and X7R ceramic capacitors were used, both being fairly common options. NP0 capacitors were used due to their stability, as their capacitance does not change when a voltage is applied. It is common to find these capacitors with values of a few nF. The X7R capacitors are highly dependent on the applied voltage, but it is easier to find larger capacitance values when compared to NP0 capacitors. When the resonant circuit was built with a PCB coil Type 1, X7R capacitors were originally used, but the system did not behave as expected. Then, the X7R capacitors were replaced with NP0 capacitors and the behavior improved.

After the resonant circuits were built, the system was completed by adding a voltage supplier to the transmitter side and a load to the receiver side. The signal going through the circuit can be measured using an oscilloscope at different nodes of the circuit. In this project however, the WPT system parameter values were measured using CATS$^{\text{TM}}$ II, a testing system developed, manufactured and marketed by nok9 AB. This system is formed by two tools: Mobile Device Tester (MDT) and Base Station Tester (BST). These tools were used because they include functionality easily accessible through a graphical user interface (GUI) to make frequency sweeps when using MDT or measure some parameters at receiver side using the oscilloscope integrated into BST.

The MDT was connected to the resonant circuit. Figure 3.15 shows the setup used. The PRx coil was connected to the BST and an external load was connected as well. The external load is variable, so different values can be chosen.

The MDT's GUI also allows the input voltage, frequency and other parameters of the input signal to be set, and it can measure the primary coil current and voltage. Like MDT, BST has a GUI where the user can change some parameters in the secondary side and it can measure and show the coil current and voltage as well as rectified current and voltage (over the load).
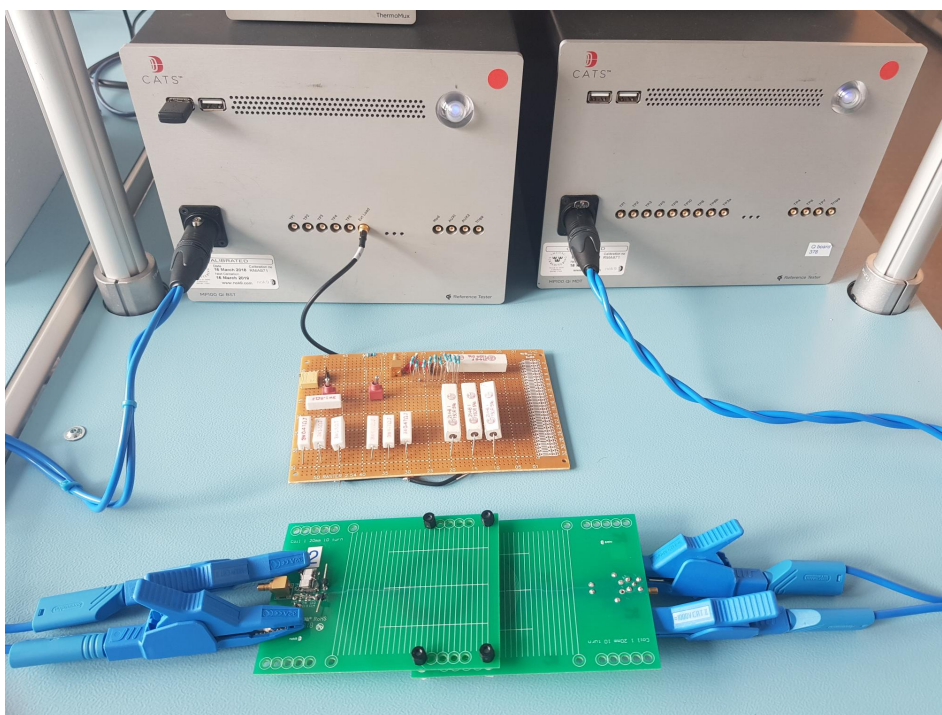
Figure 3.15: Measurement setup for WPT system parameters.

Results

This chapter presents the results obtained for the analytical, simulation and measurement work performed for this thesis. Similarly to previous chapters, it is separated into two sections. The first section contains the plots and tables built with coupling factor values and/or mutual inductance values from different scenarios, for the purpose of comparisons. These values were obtained using the developed algorithm, the simulator and the measurement tools, as described in Chapter 3. The second part presents the results from studying WPT systems. As in the first section, results from the analytical model, simulations and measurements were compared. In both sections, results are followed by short discussions about the values obtained.

4.1 Coupling factor

The coupling factor values obtained from measurements are used as the reference values to evaluate the accuracy of both the algorithm developed and the simulation software used. For a few cases measuring the values directly was impractical (e.g., single-loop coils) due to sensitivity limitation of the measurement equipment, so the analytical and simulation results were compared directly to verify that their behaviors are similar. After demonstrating the accuracy of the developed algorithm, more values are calculated using it, to study the behavior of the coupling factor in greater detail. Although the algorithm is not expected to provide the exact values (i.e., some errors exist), many coil configurations can be quickly evaluated without the need fabricate and measure them, saving both time and money.

4.1.1 Analytical approach results

To validate the algorithm, it is necessary to show the correlation between its output values and those obtained by measurement. For circular and spiral coils, 200 points were used to represent the shape of every loop, and the length of a differential segment was set as 0.01 mm. These parameters were selected after initial experimentation with the algorithm showed an acceptable speed-accuracy tradeoff, but it is not claimed here that they are optimal. Unless stated otherwise, terminals were included in the calculation. The procedure used to take measurements with real coils is explained in Section 3.1.3.

As mentioned in Section 3.1.3, two different LCR meters were used to measure the coupling factor from two identical pairs of coils for different lateral displacements (the two pairs are different from each other only due to fabrication tolerances). Figure 4.1 shows the results from one experiment, given here only as an example (hence no discussion will be provided for this case). In this plot, both the receiver and transmitter coils are Type 1 coils with 10 turns and 20 mm outer radius (for both samples 1 and 2). The different curves correspond to k measured with each LCR meter for both pairs of coils. Since the same value is measured 4 times, it is easy to detect and avoid big measurement errors.
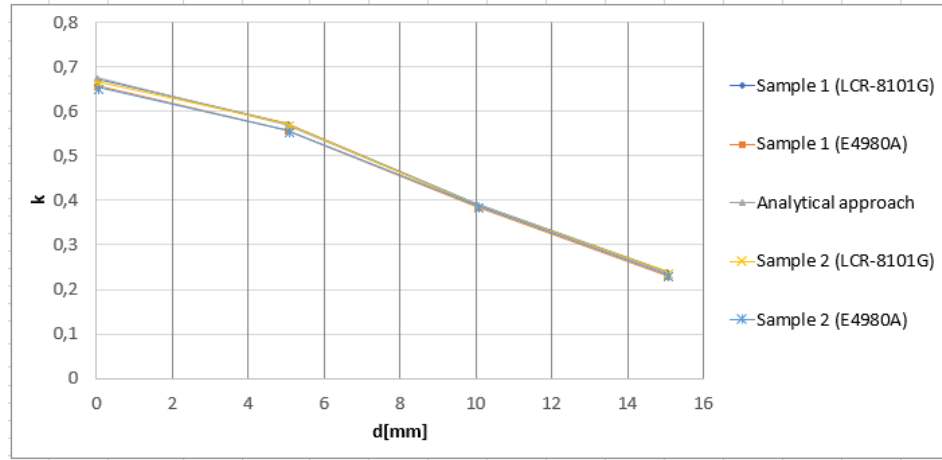
Figure 4.1: Comparison between the analytical results and the measurement results obtained with two different measurement tools and two pairs of coils (of identical type and configuration), for different lateral displacements and $h = 2.45$.

The coupling factor depends on the coils' shape and relative distance. Experiments were run in which only one of the variables was changed, to study it in isolation. Again, the values were compared with the analytical results from the algorithm.

Figure 4.2 shows the coupling factor from coils with 10 turns and 20 mm outer radius (Type 1). The graph illustrates how the coupling factor changes as a function of the lateral displacement (d) in mm. Three different scenarios are included, each one corresponding to a different vertical distance (h) value. Curves calculated using the analytical approach are compared with measurement results. To make the graph easier to understand, it includes only measurements from a single pair of coils (sample set 1) using a single LCR meter (E4980A). Based on recorded data, the worst error was around 5.66% with LCR-8101G, which corresponds to an absolute error of 0.032, and was around 5.04% (absolute error of 0.011) with E4980A. This plot can be used to analyze both the algorithm's performance and the coupling factor behavior. As can be expected, k decreases when d increases, because the receiver coil moved away from the region where the magnetic field is stronger, and hence the coupled flux became smaller. The

same happened when h was increased. The figure also shows that as the vertical distance h increases, the variation due to horizontal movement d is smaller.
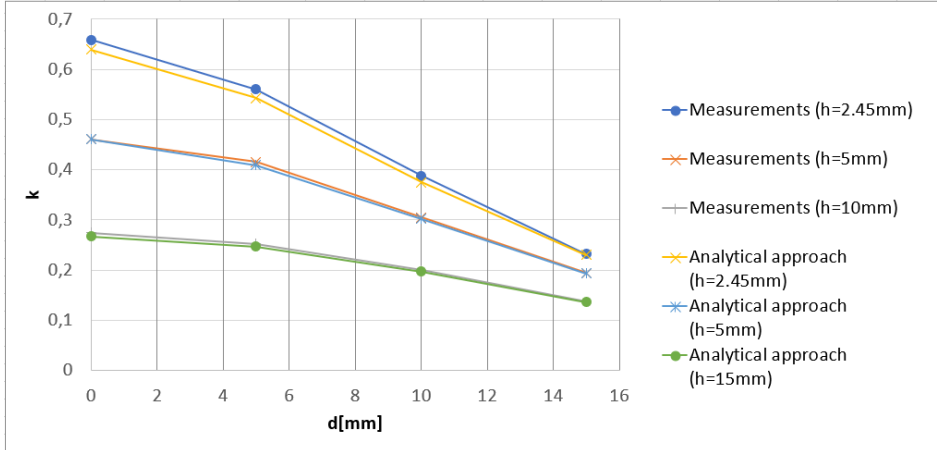
Figure 4.2: Change in k for different vertical distances (h), over different lateral displacements (d). Results from analytical approach and measurements are presented.

Figure 4.3 presents k values as a function of the vertical distance h. The PTx and PRx coils are the same. It shows results from pairs of coils with radii of 20 mm (Type 1) and 10 mm (Type 3). In both cases the coils have 10 turns. As before, only the results from a single LCR meter and a single coil pair are shown. When the radius is smaller, the coupling factor is also smaller. The difference in coupling factor decreases as h becomes larger. If this distance continues to increase, the coupling factor converges to 0 for both types of coils. As for the performance of the algorithm, it can be seen that the analytical and measured curves are in close agreement with each other. The largest error overall found for the 20 mm coils was 3.87% equivalent to an absolute error of 0.01074.In the 10 mm case, the largest overall error was as high as 22.2%, corresponding to a 0.01315 absolute error, which was obtained with the LCR-8101G. For the E4980A, the largest error of the 10 mm case was 5.14%, corrresponding to an absolute error of 0.01284.

Figure 4.4 is similar to the last one. Again, the variables under study are h and the outer coil radius. This time however, the number of turns is one. As before, the coupling factor decreases as the radius decreases. However, the analytical and measurements results differ more from each other in this scenario. This is because the lesser number of turns leads to smaller self and mutual inductances, making these values more sensitive to measurement tolerances. The biggest relative errors are 12.48% and 52.20% for the 20 mm and 10 mm coils respectively, corresponding to absolute errors of 0.0079 and 0.0178. The largest errors occur when the coils are farthest away, since at that point the k values being measured are very small, and thus there is more uncertainty in the measurements (due to limited sensitivity of the LCR meters).

The next case considered, shown in Figure 4.5, is when the PTx has a larger
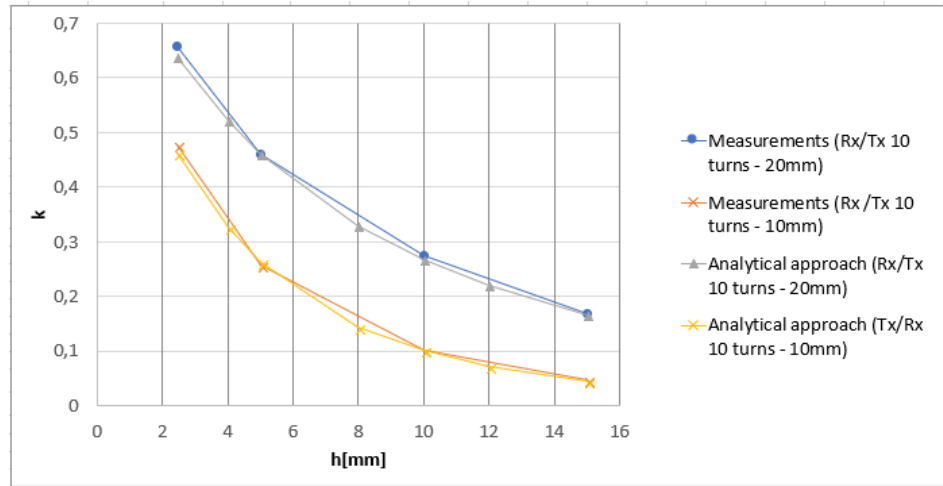
Figure 4.3: Comparison between results from analytical approach
and measurements with Type 1 (radius 20 mm) and Type 3
(radius 10 mm) coils.
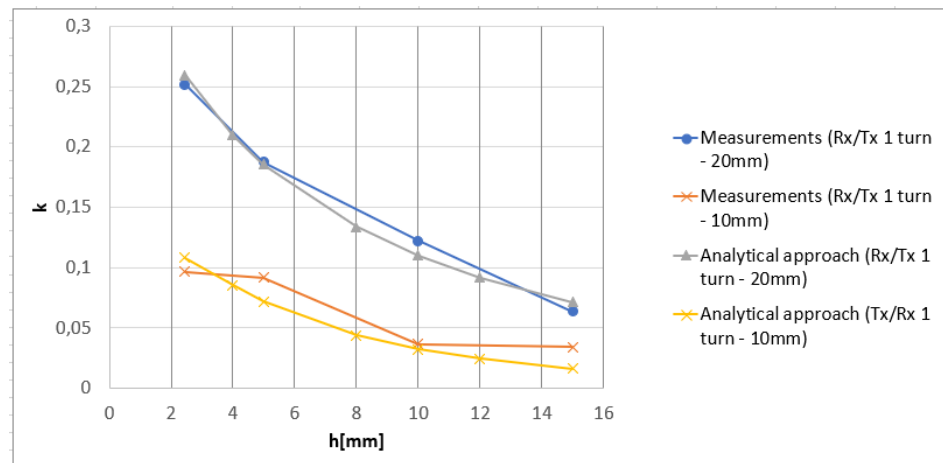
Figure 4.4: Comparison between results from analytical approach
and measurements with coils with 20 mm and 1 turn and
coils with 10 mm radius and 1 turn.

radius (20 mm, i.e., Type 1) than the PRx (10 mm, i.e., Type 3). In general, the
coupling factor decays with increasing d for different h values. However, when h
is smaller (i.e., 2.45mm) the behavior of the coupling factor as a function of d is
different. In this case the function is not decreasing monotonically. It reaches its
highest point at between 5 mm and 10 mm of lateral displacement. To explain this
phenomenon, Figures 4.6 and 4.7 show a top view of pairs of coils, where the coil
size is equal in the first one and different in the second one. If both coils have the

same size, the maximum coupling occurs when their centers coincide. When the sizes are different, the highest coupling factor occurs when the center of the smaller coil is closer to the edge of the bigger one, where the magnetic field is stronger. However, when h is increased, the magnetic field strength is again largest along the axis of the larger coil, similar to the case of similar size coils.
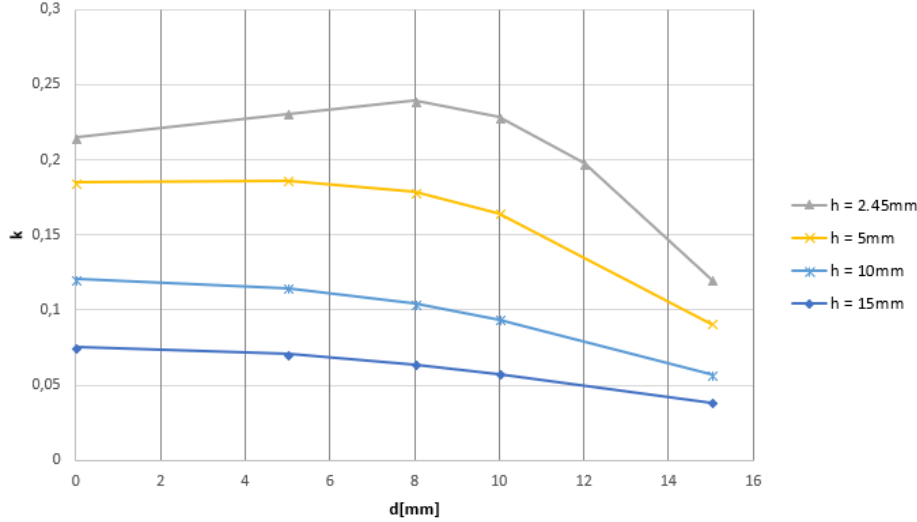
Figure 4.5: Comparison between results from analytical approach for different h values when the PTx has radius 20 mm and PRx has radius 10 mm.

(a) d = 0 mm   (b) d = 5 mm   (c) d = 10 mm   (d) d = 15 mm
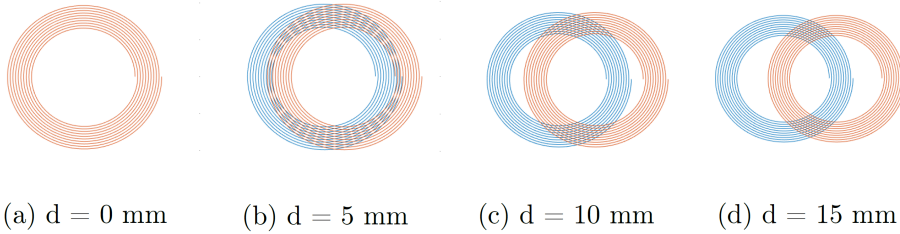
Figure 4.6: Misalignment between coils with equal dimensions.

To find out if including the terminals increased accuracy, the algorithm was run with and without them and compared to the measured values (used as reference values). Table 4.1 shows the relative errors for several values of h, for a pair of Type 1 coils with no lateral displacement. The real values were measured from a single pair of coils with E4980A. Including the terminals improves the agreement between analytical and measured results substantially when h is small (the measured values are higher), but the difference is small in the other cases.

Past research, as in [14] and [16] focused on finding formulas to calculate the

(a) d = 0 mm   (b) d = 5 mm   (c) d = 10 mm   (d) d = 15 mm
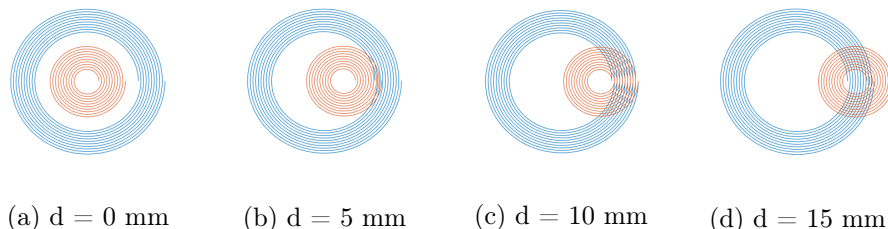
Figure 4.7: Misalignment between Type 1 and Type 3 coils.

h [mm]	Error with terminals [%]	Error without terminals [%]
2.45	0.078	2.92
5	1.21	1.25
10	2.32	2.32
15	1.09	1.08

Table 4.1: Relative error for the algorithm with and without terminals.

mutual inductance between circular coils, so the ability to calculate it on coils with other geometries is a significant improvement. To test the algorithm with non-circular coils, it was applied to a pair of square coils. The specifics of the square coils are given in Section 3.1.3. Table 4.2 presents the values calculated for two values of the vertical distance h, along with the measurements from both LCR meters. The coils were horizontally aligned (i.e., $d = 0$ and there was no rotation relative to each other). As can be seen in the table, good agreement is obtained between analytical and measurement results, especially when E4980A is used in the measurements.

4.1.2 Coupling factor in the presence of materials

Only four configurations were considered to study the effect of materials on coupling factor. Type 1 PCB coils were used both for the transmitter and receiver. In each case, a ferrite plate was placed "behind" the transmitter, on the side opposite to the receiver. Two different plate dimensions were considered, 53 mm x 53 mm and 106 mm x 106 mm. The thickness for both plates is 2.5 mm. The other parameter that was varied was the vertical separation h between the coils, both 2.45 mm and 5 mm were used. Table 4.3 shows the results of this study. As said in Section 3.1.1, the algorithm used to account for the presence of the ferrite plate (based on the method in [7]) assumes that the plate's width and length are infinite. Because of this, the calculated value is closer to the measured one when the bigger plate is used. As explained in Section 3.1.1, minor error is also expected from the algorithm not taking into account of the coil terminals in the calculation of the effect from the ferrite plate.

h [mm]	Parameter	Analytical approach	LCR-8101G			E4980A		
			Value	Error [%]	Absolute error	Value	Error [%]	Absolute error
2	M	2.79×10^{-6} H	2.65×10^{-6} H	5.32	1.41×10^{-7} H	2.70×10^{-6} H	3.21	8.67×10^{-8} H
	k	6.93×10^{-1}	6.86×10^{-1}	1.02	6.99×10^{-3}	6.84×10^{-1}	1.25	8.56×10^{-3}
5	M	1.93×10^{-6} H	1.68×10^{-6} H	14.9	2.51×10^{-7} H	1.89×10^{-6} H	1.92	3.63×10^{-8} H
	k	4.79×10^{-1}	4.29×10^{-1}	11.7	5.01×10^{-2}	4.68×10^{-1}	2.25	1.05×10^{-2}

Table 4.2: Mutual inductance (M) and coupling factor (k) calculated from a pair of square coils, with $d = 0$ mm and two h values.

Ferrite size [mm]	h [mm]	d [mm]	Analytical approach [H]	Measured value			
				LCR-8101G		E4980A	
				Error [%]	Absolute error [H]	Error [%]	Absolute error [H]
106 x 106	2.45	0	5.47×10^{-6}	0.72	3.89×10^{-8}	0.95	5.18×10^{-8}
106 x 106	5	0	4.02×10^{-6}	0.02	6.75×10^{-10}	0.29	1.16×10^{-8}
53 x 53	2.45	0	5.47×10^{-6}	1.96	1.05×10^{-7}	1.57	8.44×10^{-8}
53 x 53	5	0	4.02×10^{-6}	9.08	3.35×10^{-7}	3.27	1.27×10^{-7}

Table 4.3: Mutual inductance (M) of Type 1 coils in the presence of ferrite

4.1.3   Accuracy of simulation software

Section 3.1.2 presented several simulation models designed in Ansys Maxwell. This section shows the results of running simulations based on these models. When possible, they were compared to physical measurements. For the mutual inductance comparison of single-loop coils, obtaining good accuracy from real measurement was problematic, so for these cases the simulation results served as the reference values for comparison with the results from the analytical approach.

I) Self Inductance
As explained in Section 3.1.2, the first few models were designed to calculate self-inductance, namely one with a square coil (see Figure 3.4) and one with a two-layer coil with ferrite in the bottom (see Figure 3.5), with the two-layer coil following the dimensions of the Qi Specification. The simulations with these models were executed and the self-inductances found were compared with the values measured from the real coils. The results are shown in Table 4.4. The error in the values calculated using the simulations was around 1% of the measured values.

Coil	Simulated value [H]	Measured value [H]	Error [%]	Absolute error [H]
Square Coil	4.06×10^{-6}	4.01×10^{-6}	1.02	4.08×10^{-8}
Ferrite	2.44×10^{-5}	2.46×10^{-5}	0.76	1.88×10^{-7}

Table 4.4: Self-inductance values from Ansys Maxwell and measurements.

II) Mutual Inductance
The first cases considered for mutual inductance calculation concerned single-loop coils. Coils with 0.5 mm and 0.7 mm wire thickness were simulated. The single-loop cases are the hardest ones to validate with real measurements because the coil inductance is low and that leads to larger errors due to limited sensitivity of the LCR meters, as was already mentioned in Section 4.1.1. Therefore, the simulation results were compared with those from the algorithm instead. The results in Table 4.5 correspond to the scenario when the wire thickness is 0.5 mm, and those in Table 4.6 correspond to the scenario with the wire thickness of 0.7 mm. Although the values obtained from the analytical approach do not match completely with simulated values, the comparison allows for a quick evaluation of the usefulness of either method in providing consistent results. As can be seen, the higher the mutual inductance, the more similar both values are. However, for the range of parameters studied here, the difference is never larger than 10%.

The second set of simulations built to calculate mutual inductance used circular spiral coils (Type 1), already shown in Figure 3.7 and described in the previous chapter. The results from these simulations are presented in Table 4.7. Notice that in this particular case, the error is smaller when the mutual inductance is smaller, and the values reported by the different tools used are also closer.

h [mm]	d [mm]	Analytical approach, value [H]	Simulation approach		
			Value [H]	Error [%]	Absolute error [H]
2	0	6.00×10^{-8}	5.97×10^{-8}	0.41	2.48×10^{-10}
5	0	3.77×10^{-8}	3.66×10^{-8}	2.83	1.07×10^{-9}
10	0	2.22×10^{-8}	2.09×10^{-8}	5.96	1.32×10^{-9}
15	0	1.45×10^{-8}	1.31×10^{-8}	9.61	1.39×10^{-9}

Table 4.5: Comparison of mutual inductance between algorithm and Ansys Maxwell for single-loop cases with wire thickness of 0.5 mm.

h [mm]	d [mm]	Analytical approach, value [H]	Simulation approach		
			Value [H]	Error [%]	Absolute error [H]
2	0	6.04×10^{-8}	6.21×10^{-8}	2.85	1.72×10^{-9}
5	0	3.76×10^{-8}	3.80×10^{-8}	1.11	4.23×10^{-10}
10	0	2.13×10^{-8}	2.24×10^{-8}	4.97	1.12×10^{-9}
15	0	1.46×10^{-8}	1.33×10^{-8}	8.95	1.31×10^{-9}

Table 4.6: Comparison of mutual inductance between algorithm and Ansys Maxwell for single-loop cases with wire thickness of 0.7 mm.

Another scenario simulated in Ansys Maxwell included a metal object (an aluminium cylinder). As was explained in Chapter 3, it is necessary to use a different solver (eddy currents instead of magnetostatics) in this case. The setup applicable for both simulation and measurement is given in Section III. Table 4.8 shows the results. As it can be seen, the simulation results are closer to the measured ones when the metal object is not included. This could be caused by limitations in the simulation software, it may also happen in part due to measurement tolerances. In any case, the largest deviation between the results with the metal object is still less than 8%.

Figure 4.8 shows the results of all methods used to get the coupling factor for a pair of Type 1 of coils (20 mm, 10 turns). Note that the values from the algorithm developed during this project are slightly closer to the measured values than the simulated ones when the distance h is smaller. However, the absolute differences are small and become even smaller as h increases. The larger discrepancy of the simulated values may be due to improper modeling (i.e., geometry of the coils not reflecting that of the real coils) rather than intrinsic limitations of the simulation program.

In particular, a characteristic of the models built using the simulator is that the wires have a circular cross section. Since the real coils are built on PCB, the cross section of the conductor is rectangular, and its width and height are

h [mm]	d [mm]	Simulation approach [H]	Measured					
			LCR-8101G			E4980A		
			Value [H]	Error [%]	Absolute error [H]	Value [H]	Error [%]	Absolute error [H]
2.45	0	3.65×10^{-6}	3.39×10^{-6}	7.72	2.62×10^{-7}	3.39×10^{-6}	7.88	2.67×10^{-7}
5	0	2.45×10^{-6}	2.33×10^{-6}	4.85	1.13×10^{-7}	2.34×10^{-6}	4.40	1.03×10^{-7}

Table 4.7: Comparison of mutual inductance between results from Ansys Maxwell and measurements for Type 1 coils

		Simulation approach [H]	Measured value					
			LCR-8101G			E4980A		
		Value [H]	Value [H]	Error [%]	Absolute error [H]	Value [H]	Error [%]	Absolute error [H]
Without aluminum	M	3.32×10^{-6}	3.37×10^{-6}	1.44	4.84×10^{-8}	3.37×10^{-6}	1.40	4.72×10^{-8}
Without aluminum	k	6.67×10^{-1}	6.69×10^{-1}	0.31	2.07×10^{-3}	6.55×10^{-1}	1.82	1.20×10^{-2}
With aluminum	M	2.54×10^{-6}	2.36×10^{-6}	7.85	1.85×10^{-7}	2.35×10^{-6}	7.96	1.87×10^{-7}
With aluminum	k	5.75×10^{-1}	5.60×10^{-1}	2.65	1.48×10^{-2}	5.53×10^{-1}	4.04	2.23×10^{-2}

Table 4.8: Simulations and measurements without and with a metal object in the two-coil configuration.
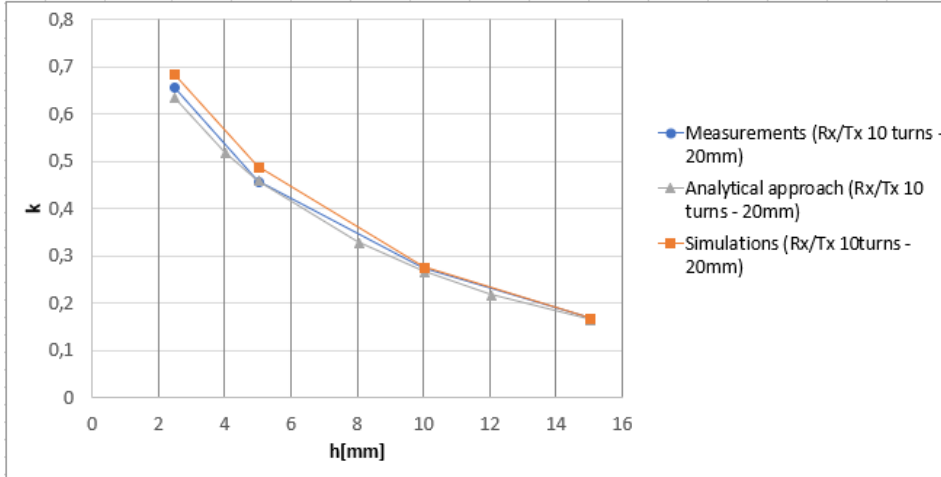
Figure 4.8: Comparison between results from analytical approach,
measurements and simulations with coils with 20 mm radius
and 10 turns (Type 1 coil).

restricted to certain values. An assumption commonly used is that the current
density is constant. For this to hold, the ratio of width to height should be 1:1,
but the manufacturer could deliver coils with a ratio of 5:2 at best. This could
cause some of the differences in the results shown.

4.2   WPT

After focusing on the couple factor in the previous section, this section examines
other important parameters of WPT systems. A WPT system is analyzed as an
electrical circuit. As in the previous study of inductances and coupling factor,
three different approaches were used.

4.2.1   Load voltage (V_L) variation with coupling factor (k)

Figures 4.9, 4.10 and 4.11 show the load voltage as a function of frequency for
different relative positions between the PTx and PRx coils (and thus different
coupling factors). Measurements were taken from pairs of coils of the same size
(Type 1 coils) and of different sizes (Type 1 and Type 3 coils). Note that the
printed coils on the two PCBs faced each other at $h = 0$ mm and $d = 0$ mm and
the coil surfaces were only separated by protective laminates of thickness 0.01 mm.
      Notice that the voltage is always higher when the coupling factor is higher.
In general, the coupling factor increases when the PTx and PRx coils are placed
closer to each other and are well aligned to each other. The increase does not
appear to be constant, since the curves have slightly different shapes. However,

they are not intersecting in the given frequency range, which means that increasing the coupling factor reliably increases voltage.
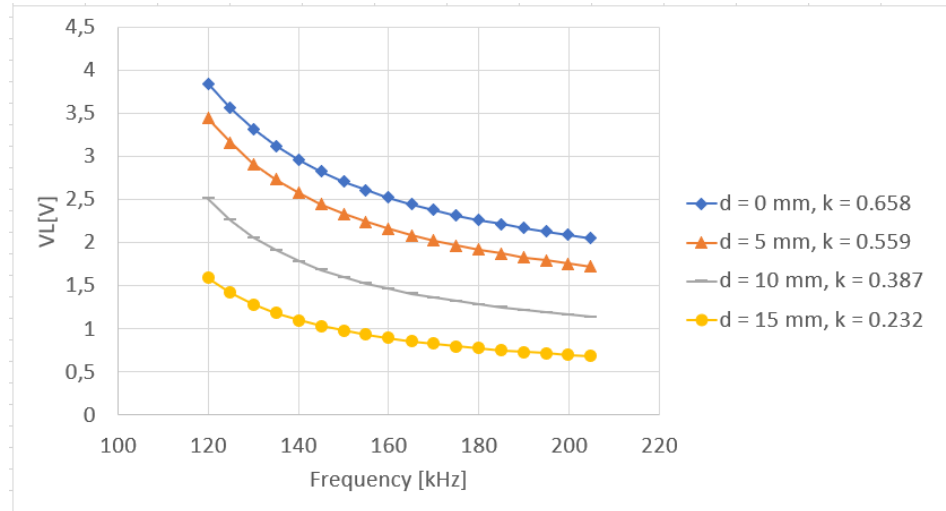

Figure 4.9: Load voltage for coils of the same size with vertical distance (h) equals to 2.45 mm for different lateral displacement (d) values.
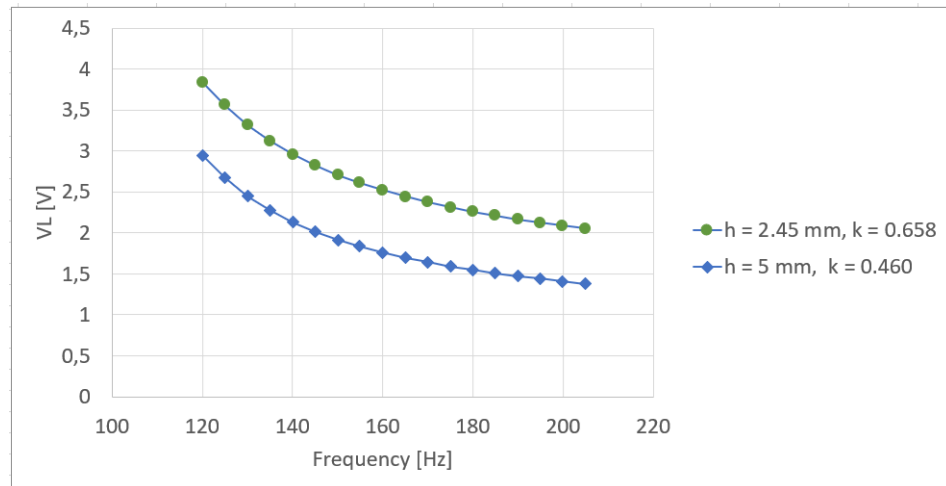

Figure 4.10: Load voltage for coils of the same size with lateral displacement (d) equals to 0 mm for different vertical distance (h) values.

If only the h value is changed, the coupling factor has the same behavior for both similar and different PTx and PRx coils. The further away the coils are, the smaller the coupling and the load voltage. On the other hand, lateral displacement
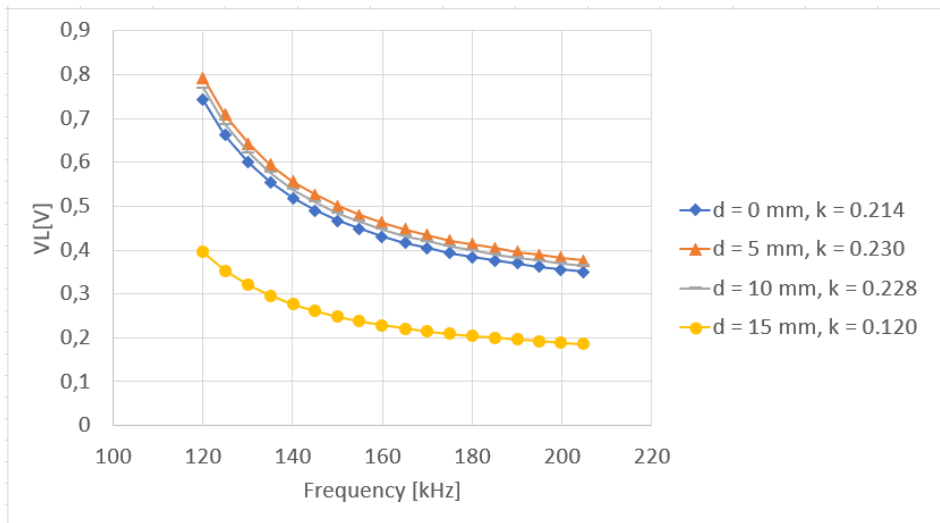
Figure 4.11: Load voltage for coils of different sizes with vertical distance (h) equals to 2.45 mm for different lateral displacement (d) values.

d between similar PTx and PRx coils provides a monotonic decrease in coupling and hence load voltage, whereas dissimilar PTx and PRx can show a different behavior of coupling and load voltage over d depending on the h value (as seen in Figure 4.5 as well as Figure 4.11. In short, the load voltage follows closely the behavior of the coupling factor.
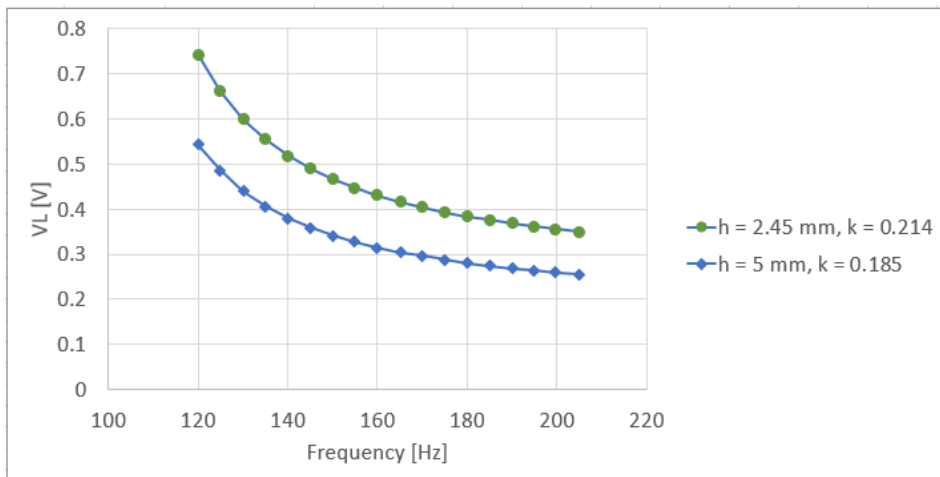

Figure 4.12: Load voltage for coils of different sizes with lateral displacement (d) equals to 0 mm for different vertical distance h values

Analytical and simulation methods to calculate WPT system parameter values
were described in Section 3.2. The results obtained from those methods are shown
in Figures 4.13 and 4.14. As it can be seen from the plots, both the simulations and
the algorithm are more in agreement with the measurements when the frequency
is higher. Note that the results from the analytical and simulation approaches are
more similar when compared to each other than when compared to the measured
values. This is plausible as they are likely applying the same equations for the
calculations. The difference observed when comparing to the real measurements
at lower frequencies (close to the resonant frequency) is caused by the components'
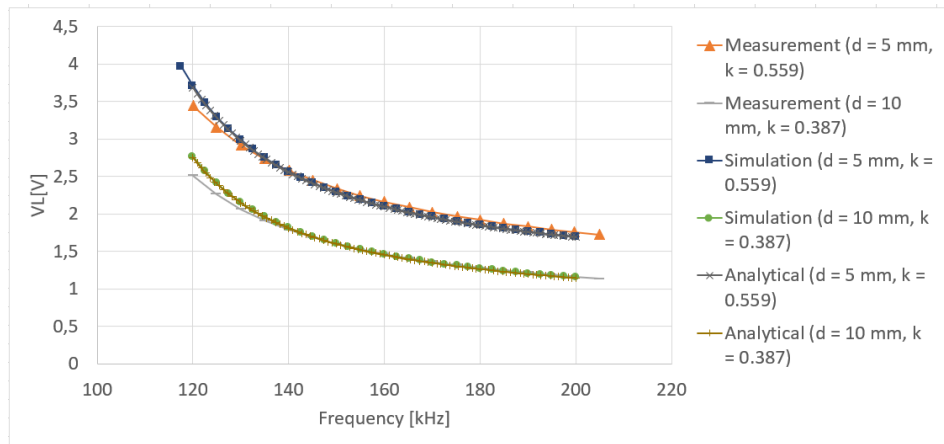resistance, which increases when currents flow through them.

Figure 4.13: Comparison between the results from each approach
used in this project. Load voltage for coils of different sizes
with vertical distance (h) equals to 2.45 mm for different
lateral displacement (d) values.

4.2.2   Primary coil current (I_p) variation with coupling factor (k)

Figures 4.15 and 4.16 show the measured primary current values. The measure-
ments were done on Type 1 coils as PTx and PRx. For low frequencies, the primary
current decreases as the coupling factor increases, but for high frequencies the op-
posite is true.

The primary side coil current is given by $I_p = V_{in}/Z_p$. Since the input voltage
was the same for all the measurements, the different behaviors seen in the figures
must be caused by the impedance seen by the primary side, Z_p. As in Section
2.1.1, Z_p is a function of both the coupling factor k and the impedance of the
secondary side Z_s. According to data collected using the analytical approach, the
imaginary part of Z_s changes its sign in observed range of frequencies from negative
to positive (i.e., the reactance goes from capacitive to inductive). This triggers the
change in the behavior of Z_p (and I_p) as a function of k: for lower frequencies Z_p
increases when k increase; for higher frequencies, Z_p increases when k decreases.
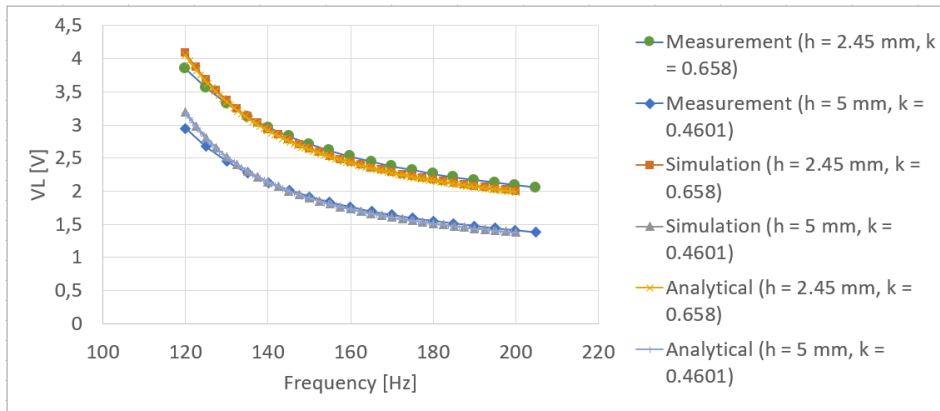The different curves intersect each other due to this change in impedance.

Figure 4.14: Comparison between the results from each approach used in this project. Load voltage for coils of the same size with lateral displacement (d) equals to 0 mm for different vertical distance (h) values.
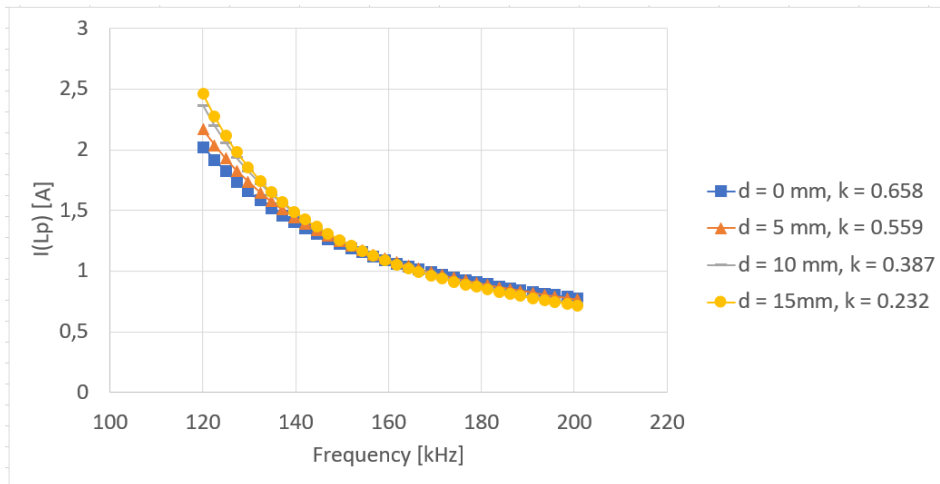

Figure 4.15: Primary coil current for coils of the same size with vertical distance (h) equals to 2.45 mm for different lateral displacement (d) values.

4.2.3   Primary coil current (I_p) variation with load (Z_L)

The primary coil current increases when the load increases for frequencies close to resonant frequency, as seen in Figure 4.17. This may be caused by a change in the behavior of the real components when the frequency is close to the resonant frequency. For frequencies farther away from that point, the primary coil current is lower when the resistance is larger. Again, measurements were done using Type 1 PTx and PRx coils. Further study using the analytical model showed that for
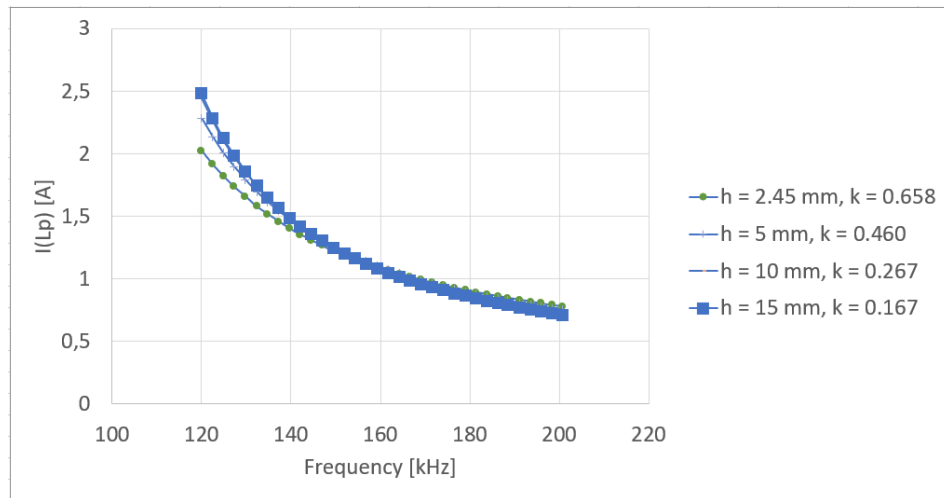
Figure 4.16: Primary coil current for coils of the same size with lateral displacement (d) equals to 0 mm for different vertical distance (h) values.

the frequency values at which the primary coil currents coincide, the impedances seen by the primary side coil also coincide.
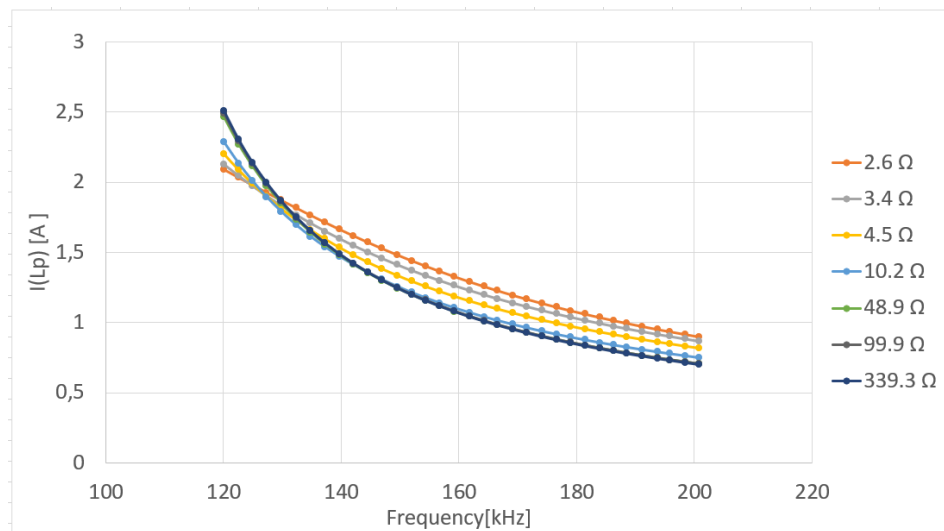

Figure 4.17: Primary coil current for different load values.

4.2.4 Sensitivity

Initially, a problem occurred while building the measurement setup due to the use of low quality capacitors, as mentioned in Section 3.2.3. Figure 4.18 shows how the current in the transmitter changes by changing the type of capacitor. The circuit is more selective (i.e., the curve is steeper) when higher-quality NP0 capacitors are used. Note that all measurements in this section were done on Type 1 PTx and PRx coils.

   Electronic components can have small factory defects, and measurement tools also introduce errors. Problems with some components encountered during the course of this project raised the question of how sensitive WPT systems are to changes in specific parameters, in order to find out if these small errors could affect system performance. Figures 4.19 to 4.23 show how the load voltage changes when the values for specific parameters vary between $\pm 5\%$ of the parameters' nominal values. Since the results presented in the previous sections show that the WPT system analytical model is reasonably accurate, it was used to generate the data for these plots. This way the parameter values could be easily changed.
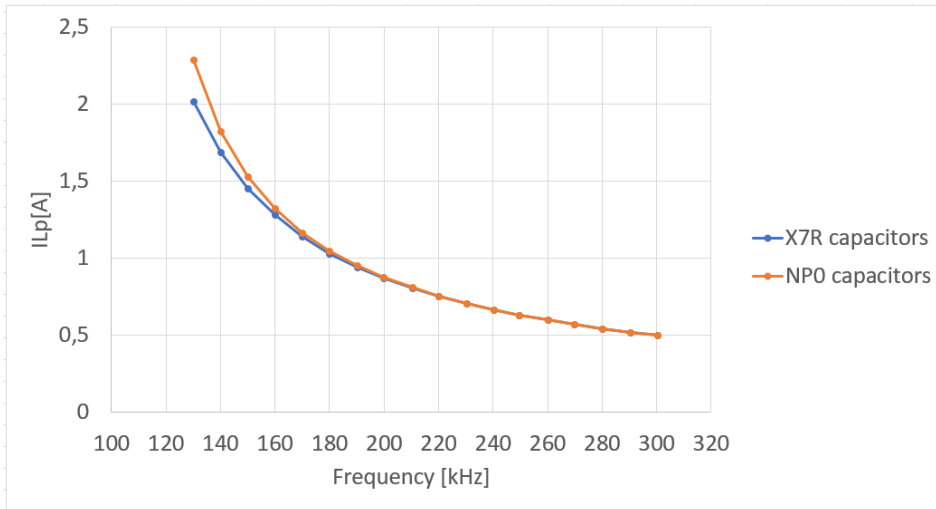

Figure 4.18: Current in the transmitter side with X7R and NP0 capacitors.

   Figure 4.19 shows the load voltage when L_p varies. These curves have similar shapes but the resonant frequency decreases as L_p increases. Varying C_p causes a similar effect, as can be seen in Figure 4.20.

   When L_s varies the change in the load voltage is observed in Figure 4.21 to be smaller than the one caused by modifying L_p. In this case, the resonant frequency does not change, but the bell-like part of the curve gets slightly wider as L_s increases. Using simulations and the analytical model it can be verified that the stronger sensitivity towards L_p occurs even when $L_s \leq L_p$. However, this may be due to the fact that the equivalent model introduces a new variable L_m (the magnetizing inductance) that depends on L_p but not on L_s. On the other hand,

Figure 4.19: Load voltage for coils of the same size with lateral displacement (d) equals to 0 mm and vertical distance (h) equals to 2.45 mm for different values of L_p in the range $\pm 5\%$ of its nominal value.

Figure 4.20: Load voltage for coils of the same size with lateral displacement (d) equals to 0 mm and vertical distance (h) equals to 2.45 mm for different values of C_p in the range $\pm 5\%$ of its nominal value.

if C_s changes in the $\pm 5\%$ range, no significant change in the load voltage occurs (see Figure 4.22).
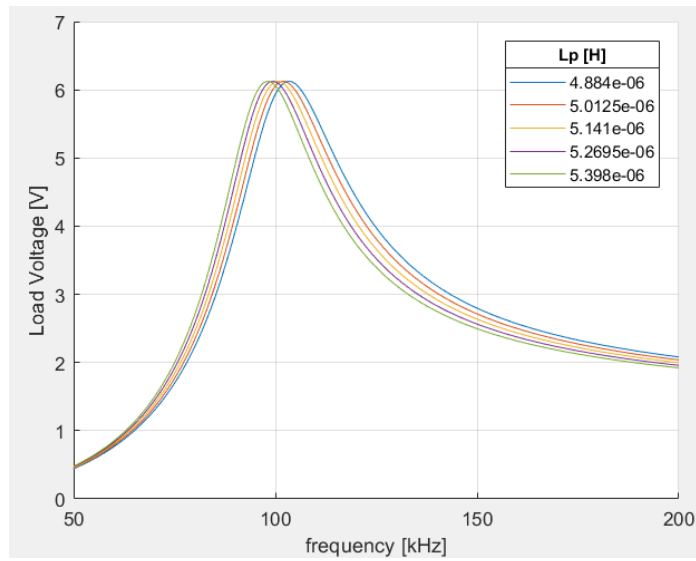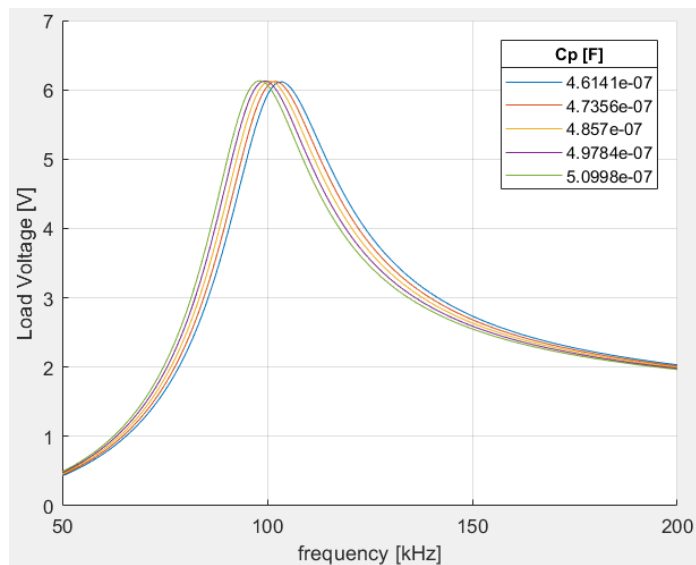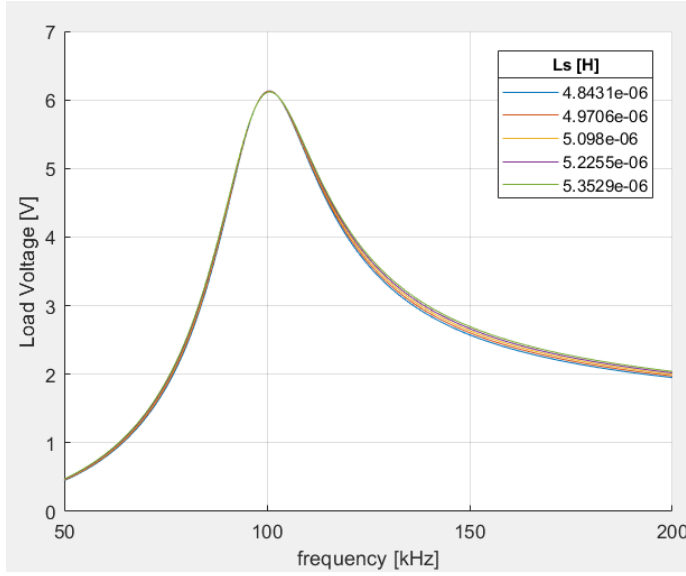

Figure 4.21: Load voltage for coils of the same size with lateral displacement (d) equals to 0 mm and vertical distance (h) equals to 2.45 mm for different values of L_s in the range $\pm 5\%$ of its nominal value.

A change in the load Z_L within the considered $\pm 5\%$ range of its nominal value does not produce significant changes in the load voltage, as shown in Figure 4.23. However, the maximum amplitude increases slightly as the load increases, which also leads to a slightly steeper slope and hence a slightly higher Q value.

It is well known that the performance of WPT systems heavily depends on the coupling factor, and by extension on all the variables that are used to determine it. However, small scale changes in k do not cause abrupt changes in the load voltage, as can be seen in Figure 4.24. As in the case of L_s, only the width of the bell-like curves varies slightly with k. The data generated shows that, in these particular cases, when only small variations of 5% or less of the nominal value are considered, WPT performance is more sensitive to changes in the primary side parameters C_p and L_p than to changes in L_s, C_s, Z_L or even k.

4.2.5   Resonance split frequency

The following parameters were used in the method developed to study the resonance split frequency explained in Section 3.2.1.

$V_{in} = 2.45$ V, $C_p = 0.486$ μF, $L_p = 5.141$ μH, $R_p = 0.391$ Ω, $C_s = 0.491$ μF, $L_s = 5.10$ μH, $R_s = 0.396$ Ω.

Figure 4.25 shows the primary coil current calculated using the above parameters and k equals to 0.658. In the plot, resonance split starts to occur at around
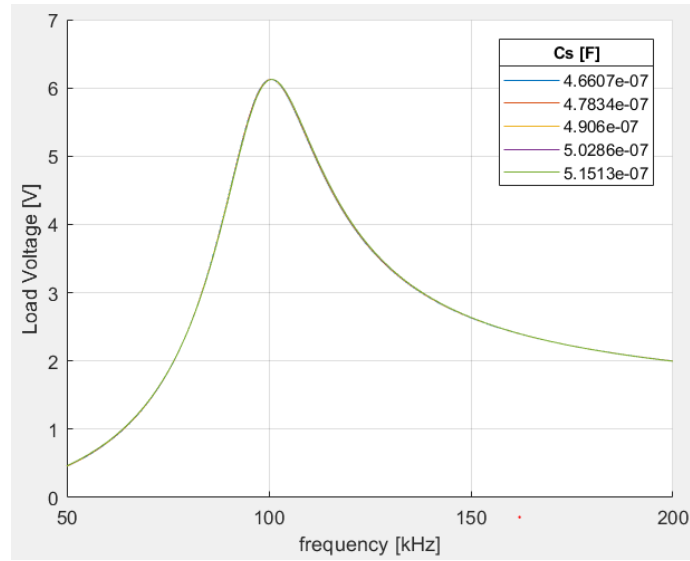
Figure 4.22: Load Voltage for coils of the same size with lateral
displacement (d) equals to 0 mm and vertical distance (h)
equals to 2.45 mm for different values of C_s in the range $\pm 5\%$
of its nominal value.

a load of 2 Ω. The developed script returns 2.36 Ω as the smallest value where
resonance split does not happen. Figure 4.26 shows the primary coil current for
a similar set of parameters, but when the coupling factor takes the lower value
of 0.388. In this case, the minimum load value before the resonance split phe-
nomenon appears is lower, i.e., 1.26 Ω (obtained according to the method used).
This matches the notion that if the coupling is very low then the load will hardly
affect the transmitter side, because both circuits will work as independent systems.
This result also demonstrates that it is not possible to determine the starting point
for resonance split based only on L_s, C_s, L_p and C_p, because if k changes that point
will also change. Analytically, the derivative used to find the number of peaks in
the function includes all of these parameters, so the positions of the maxima and
minima also depend on all of them.

Figure 4.23: Load Voltage for coils of the same size with lateral displacement (d) equals to 0 mm and vertical distance (h) equals to 2.45 mm for different values of Z_L in the range $\pm 5\%$ of its nominal value.
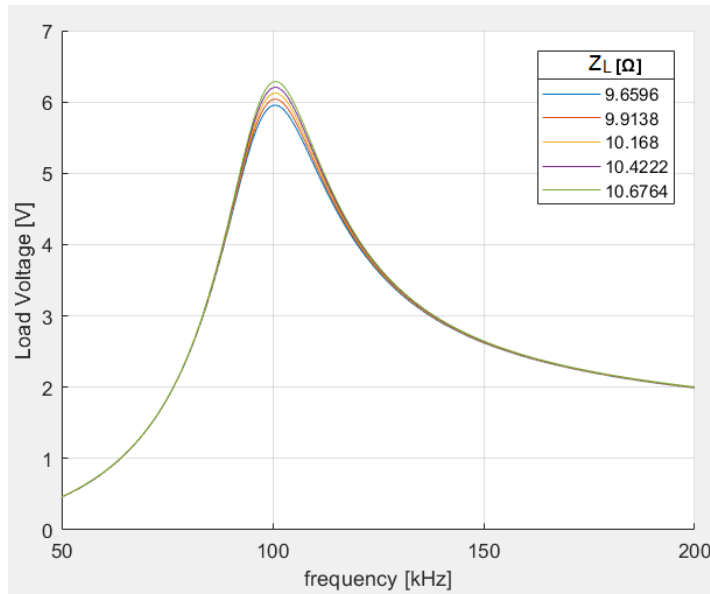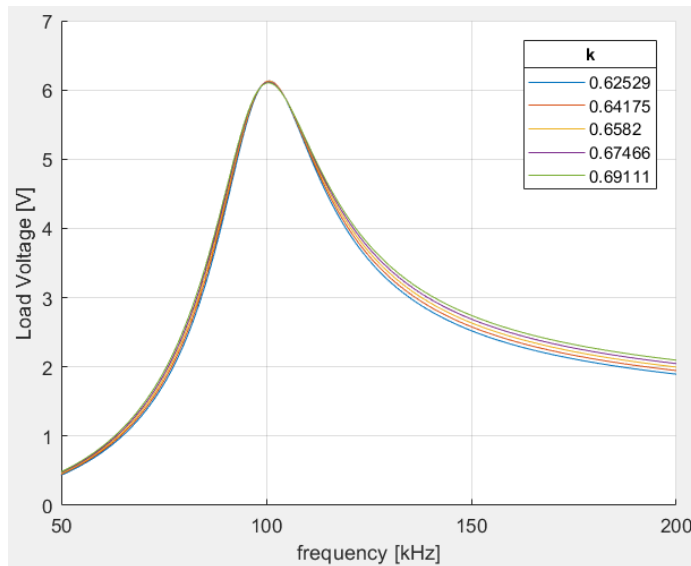

Figure 4.24: Load voltage for coils of the same size with lateral displacement (d) equals to 0 mm and vertical distance (h) equals to 2.45 mm for different values of k in the range $\pm 5\%$ of its nominal value.
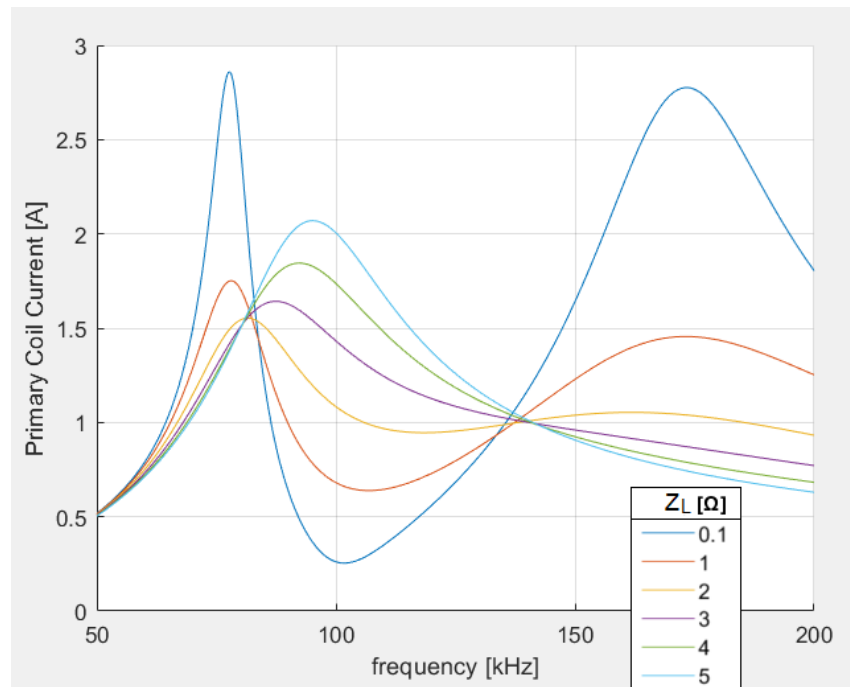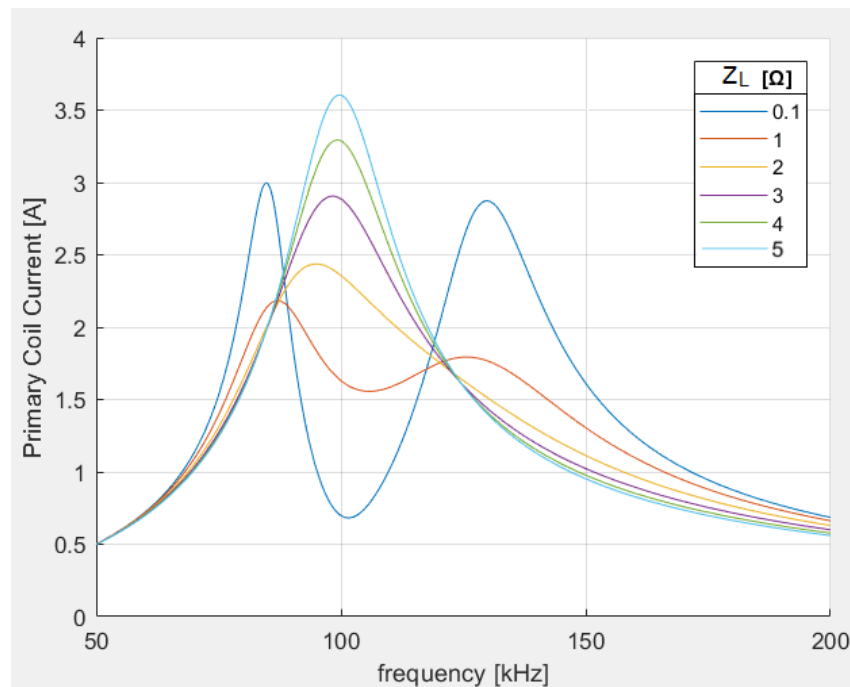
Figure 4.25: Resonance split phenomena when $k = 0.658$.

Figure 4.26: Resonance split phenomena when $k = 0.388$.

Conclusions and Future Work

5.1 Conclusions

One of the goals of this project was to study how accurate commercially available electromagnetic simulation programs are for modeling WPT systems. The simulator selected to model and simulate WPT coils proved to be useful to analyze different parameters such as self inductance, mutual inductance and coupling factor. By using the Eddy currents solver a more in depth study is possible, since more variables can be taken into account, like frequency and Eddy current losses. The presented results show that the simulator is an appropriate tool to study alternative system designs and components without having to manufacture prototypes. However, when deciding between software such as Ansys Maxwell and other approaches (like the algorithms developed based on an analytical model) many factors have to be taken in account. Commercial software tends to be expensive. Furthermore, running simulations on more general-purpose electromagnetic simulation software tends to be computationally intensive and can take a long time.

For its part, the algorithm developed to calculate the coupling factor based on the analytical model showed good agreement with other approaches in the cases considered. Note however that this approach relies on several assumptions. The dependency on frequency is ignored, and the current path is taken as a filament in the middle of the wire. Self-inductance has to be numerically approximated, which adds another source of errors. The current algorithm is also not able to consider objects surrounding the coils. Circular coils (or any coils with non-straight sections) are approximated using a discrete sequence of points, and the number of points used can affect the results. This problem does not occur with geometries that can be accurately described with straight line segments, where it is only necessary to specify the starting and ending points. Still, the results obtained were satisfactory. This analytical approach is more limited when it comes to dealing with a more general coil setup, due to the aforementioned assumptions, but for its specific purposes it offers a more efficient alternative when compared to using a full blown electromagnetic, both in cost and in computation time. For comparison, calculating the mutual inductance between two Type 1 coils takes 55 minutes in Ansys Maxwell and around one and a half minutes using the analytical method presented in this report.

As for the behavior of the coupling factor, as expected it proved to be very sensitive to the relative positions of the transmitter and receiver. When both coils are the same size, the coupling factor is almost halved if the lateral misalignment is close to half of their outer radius, when the vertical distance is fixed at 2.45 mm. An increase in vertical distance from 2.5 mm to 5 mm reduces the factor by around 20%, with no laternal misalignment. However, the results also show that an increase in lateral misalignment does not necessarily imply a smaller coupling factor. The effect lateral displacement has depends on the relative dimensions of the coils. Although fewer scenarios were designed to study how the coupling factor is affected by the presence of metal plates, the few tests carried out show that both Ansys Maxwell and methods from previous works can handle these scenarios with reasonable accuracy, at least for the case of ideal circular coils.

The simple analytical model for WPT systems was shown to offer reasonable accuracy, taking the measurements done as the reference values. Therefore, the corresponding equations can be used to describe the relationship among the parameters and predict their behavior. Similarly, LTspice proved to be a useful, easy to use tool. A single model can be easily used to generate data for several different values of its input parameters. Its waveform viewer enables quick visualization of the circuit's AC signal at the desired points. It can be concluded from the results that the load voltage versus frequency curves have a similar shape for different coupling factors, the difference being that the curves are effectively frequency translated versions of one another. The measured load voltage results match the observed behavior of the coupling factor from simulations. On the other hand, the shape of the primary coil current changes more significantly when the coupling factor varies. Both the coupling factor and the load affect how narrow the bell-like curve is, indicating their effect on the Q factor of the WPT circuit.

An important practical aspect of WPT systems found during this project is the importance of choosing appropriate components and knowing how they behave under the conditions of interest. There will always be small differences between components that should have similar characteristics due to design limitations and manufacturing tolerances. But this must be checked and kept under control, because small modifications in some parameters can greatly affect system performance.

The results from this project support the need to have a standard that specifies the characteristics of each part of a WPT system. Small variations in coil alignment, coil size or the distance between coils (which originates for example from the protective cover of a mobile phone), and the materials used by devices that use WPT, can have a significant impact on the coupling between the transmitter and receiver. Therefore, they affect the performance of the whole system.

Different tools can be used to to analyze these systems. During this project we have verified that both the simulators used (Ansys Maxwell and LTspice) and the mathematical models used to analytically calculate values are coherent with collected measurements. These tools can be of great value in a field where prototyping can be time consuming and measurements are noisy.

5.2   Future work

Understand the behavior of the variables in inductive coupling WPT systems and how they interact with one another was one of the objectives of the thesis project. Due to time constraints, the number of variables included and the complexity of these systems, many ideas where left out and can serve as the starting point for future projects. For example, the algorithm to calculate the coupling factor can be improved. One could try to find the optimal number of points needed to describe certain geometric shapes. It can be extended to handle non constant current densities. Another option is to try to model the effect of the different types of wires commonly used to manufacture coils. The method can be further validated with test cases including new geometrical shapes. It can also be used to find equations to calculate the coupling factor for specific shapes, by generating enough data to fit a function to it.

This project only considered one case regarding the use of ferrite plates. Specifically, it considers when a ferrite plate is placed behind one of the coils (i.e., not the side facing the other coil). The authors of [19], who came up with the analytical formula for the single-ferrite case, have also extended it to handle the case with ferrites behind the other coil as well. The code written could be extended to include this new functions. Another possible area of improvement would be to try to extend these functions to handle materials between the transmitter and receiver or in other positions and then analyze how this affects the coupling factor. This would be especially interesting due to the current need to increase the efficiency of WPT systems and the fact that mobile phones contain metal parts that can affect performance. It would also be useful to find equations like the ones in [19] for other geometries, since those are designed for circular coils.

During the analysis of WPT systems, many interesting observations were made. The mathematical equations and the relationship among the variables were verified. The sensitivity of certain circuit components within the system was observed, and knowing beforehand which parameters are more delicate can help the design of transmitters and receivers. But there are many other useful studies to be done. An example is the study of the split resonant frequency phenomenon. It was not possible to find a closed form function to calculate at which point it starts happening. From a completely analytical point of view, the researcher can try to find solutions for the polynomial expression found, or at least a way to count its stationary points.

As explained in Section 2.1, real WPT systems have a complex structure. For this project it was decided to use a simplified model, where neither the converter nor the rectifier circuit was considered. A logical next step would be to model these elements as a function of frequency and add them to the models used in this project. If this is achieved, the load voltage can be calculated more accurately.

References

[1] C. D. J.-P. Curty, M. Declercq and N. Joehl., *Design and Optimization of Passive UHF RFID Systems.* Boston, USA: Springer US, 2007.

[2] W. Brown, "The history of wireless power transmission," *Solar Energy*, vol. 56, pp. 3–21, 1996.

[3] J. Lin, "Wireless power transmission: From far-field to near-field," Gainesville, Florida USA. [Online]. Available: http://ewh.ieee.org/r8/nor way/ap-mtt/files/Lin_WPT.pdf (Accessed 2018-08-18).

[4] Wireless power consortium. [Online]. Available: https://www.wirelesspower consortium.com/ (Accessed 2018-08-18).

[5] D. V. Wageningen and E. Waffenschmidt. Inductive power transmission. Wireless Power Consortium. [Online]. Available: https://www.wir elesspowerconsortium.com/technology/basic-principle-of-inductive-power-tr ansmission.html (Accessed 2018-08-18).

[6] E. Waffenschmidt. Resonant coupling. [Online]. Available: https://www.wirelesspowerconsortium.com/technology/resonant-coupling.html (Accessed 2018-08-18).

[7] A brief history of the Qi specification. Wireless Power Consortium. [Online]. Available: https://www.wirelesspowerconsortium.com/developers/specification.html (Accessed 2018-08-18).

[8] K. Siddabattula, "Why not a wire?" Texas Instruments, Presentation. [Online]. Available: https://www.wirelesspowerconsortium.com/data/downloadables/1/4/8/7/why-not-a-wire-the-case-for-wireless-power-kalyan-siddabattula-michigan-sept-2015.pdf (Accessed 2018-08-18).

[9] T. Brander, A. Gerfer, B. Rall, and H. Zenkner, *Trilogy of Magnetics.* Max-Eyth-Str. 1, Waldenburg, Germany: Würth Elektronik eiSos GmbH & Co. KG, 2009.

[10] L. Swaans, "Research report - modeling of a generic wpt system," nok9 A. B., Tech. Rep., 2017, internal document.

[11] N. Mohan, T. M. Undeland, and W. P. Robbins, *Power Electronics.* United States of America: John Wiley & Sons, Inc., 2003.

[12] E. Waffenschmidt. Qi coupling factor. Wireless Power Consortium. [Online]. Available: https://www.wirelesspowerconsortium.com/technology/coupling-factor.html (Accessed 2018-08-18).

[13] Y. P. Su, X. Liu, and S. Y. R. Hui, "Mutual inductance calculation of movable planar coils on parallel surfaces," *IEEE Transactions on Power Electronics*, vol. 24, no. 4, pp. 1115–1123, April 2009.

[14] M. Soma, D. C. Galbraith, and R. L. White, "Radio-frequency coils in implantable devices: Misalignment analysis and design procedure," *IEEE Transactions on Biomedical Engineering*, vol. BME-34, no. 4, pp. 276–282, April 1987.

[15] F. W. Grover, *Inductance Calculations: Working Formulas and Tables*. New York, USA: Dover Publications, Inc., 1962.

[16] S. I. Babic and C. Akyel, "New analytic-numerical solutions for the mutual inductance of two coaxial circular coils with rectangular cross section in air," *IEEE Transactions on Magnetics*, vol. 42, no. 6, pp. 1661–1669, June 2006.

[17] A. Russell, "The magnetic field and inductance coefficients of circular, cylindrical, and helical currents," in *Proceedings of the Physical Society of London*, vol. 20, no. 1, 1906, p. 476.

[18] W. G. Hurley and M. C. Duffy, "Calculation of self and mutual impedances in planar magnetic structures," *IEEE Transactions on Magnetics*, vol. 31, no. 4, pp. 2416–2422, July 1995.

[19] W. G. Hurley and M. C. Duffy, "Calculation of self- and mutual impedances in planar sandwich inductors," *IEEE Transactions on Magnetics*, vol. 33, no. 3, pp. 2282–2290, May 1997.

[20] What is matlab? The MathWorks, Inc. [Online]. Available: https://se.mathworks.com/discovery/what-is-matlab.html (Accessed 2018-08-18).

[21] Matlab documentation. The MathWorks, Inc. [Online]. Available: https://se.mathworks.com/help/matlab/ (Accessed 2018-08-18).

[22] E. W. Weisstein. Archimedean spiral. Wolfram Research. From Mathworld – A Wolfram Web Resource. [Online]. Available: http://mathworld.wolfram.com/ArchimedeanSpiral.html (Accessed 2018-08-18).

[23] Ansys > products > electromagnetics. Ansys, Inc. [Online]. Available: https://www.ansys.com/products/electronics (Accessed 2018-08-18).

[24] Members of the Wireless Power Consortium, *Introduction to the Power Class 0 Specification*, Wireless Power Consortium Std. 1.2.3, 2017.

[25] B. Hesterman, "Analysis and modeling of magnetic coupling," Discovery Learning Center, University Of Colorado, Boulder, Colorado USA, 2007. [Online]. Available: http://denverpels.org/Downloads/Denver_PELS_20070410_Hesterman_Magnetic_Coupling.pdf (Accessed 2018-08-18).

[26] Transfer functions. The MathWorks, Inc. [Online]. Available: https://se. mathworks.com/help/control/ug/transfer-functions.html (Accessed 2018-08-18).

[27] Bode. The MathWorks, Inc. [Online]. Available: https://se.mathworks.com/ help/ident/ref/bode.html (Accessed 2018-08-18).

[28] LTspice. Analog Devices, Inc. [Online]. Available: http://www.analog. com/en/design-center/design-tools-and-calculators/ltspice-simulator.html (Accessed 2018-08-18).

[29] "LTspice IV getting started guide," Linear Technology, 2011. [Online]. Available: http://www.analog.com/media/en/simulation-models/spice-models/ LTspiceGettingStartedGuide.pdf?modelType=spice-models (Accessed 2018-08-18).

[30] M. Engelhardt, "Using transformers in LTspice/SwitcherCAD III," *Linear Technology Magazine*, pp. 23–24, September 2006.